LEVEL II

U. of Iowa 78-36

Department of Physics and Astronomy

THE UNIVERSITY OF IOWA

Iowa City, Iowa 52242

(14)

U. of Iowa-78-36

(2) LEVEL II

AD A067612

DDC FILE COPY

(6)

Intense Electrostatic Waves Near the Upper Hybrid Resonance Frequency

by

(10)

W. S. Kurth, J. D. Craven, L. A. Frank and D. A. Gurnett

(11)

October, 1978

(12) 44 p.

Department of Physics and Astronomy
The University of Iowa
Iowa City, Iowa 52242

Submitted to the Journal of Geophysical Research.

The research at the University of Iowa was supported by the National Aeronautics and Space Administration through Contracts NAS1-13129, NAS5-11074, Grant NGL-16-001-043, and by the U. S. Office of Naval Research through Contract N00014-76-C-0016.

(15) NAS1-13129

188460

UNCLASSIFIED

SECURITY CLASSIFICATION OF THIS PAGE (When Data Entered)

REPORT DOCUMENTATION PAGE		READ INSTRUCTIONS BEFORE COMPLETING FORM
1. REPORT NUMBER U. of Iowa 78-36	2. GOVT ACCESSION NO.	3. RECIPIENT'S CATALOG NUMBER
4. TITLE (and Subtitle) Intense Electrostatic Waves Near the Upper Hybrid Resonance Frequency		5. TYPE OF REPORT & PERIOD COVERED Progress, October, 1978
		6. PERFORMING ORG. REPORT NUMBER
7. AUTHOR(s) W. S. Kurth, J. D. Craven, L. A. Frank, and D. A. Gurnett		8. CONTRACT OR GRANT NUMBER(s) N00014-76-C-0016
9. PERFORMING ORGANIZATION NAME AND ADDRESS Department of Physics and Astronomy The University of Iowa Iowa City, IA 52242		10. PROGRAM ELEMENT, PROJECT, TASK AREA & WORK UNIT NUMBERS
11. CONTROLLING OFFICE NAME AND ADDRESS Office of Naval Research Arlington, VA 22217		12. REPORT DATE October, 1978
		13. NUMBER OF PAGES 75
14. MONITORING AGENCY NAME & ADDRESS(if different from Controlling Office)		15. SECURITY CLASS. (of this report) UNCLASSIFIED
		15a. DECLASSIFICATION/DOWNGRADING SCHEDULE

16. DISTRIBUTION STATEMENT (of this Report)

Approved for public release; distribution is unlimited.

17. DISTRIBUTION STATEMENT (of the abstract entered in Block 20, if different from Report)

18. SUPPLEMENTARY NOTES

To be published in J. Geophys. Res., 1979

19. KEY WORDS (Continue on reverse side if necessary and identify by block number)

Electrostatic Waves
Upper Hybrid Resonance Frequency

20. ABSTRACT (Continue on reverse side if necessary and identify by block number)

[See page following.]

DD FORM 1 JAN 73 1473 EDITION OF 1 NOV 65 IS OBSOLETE
S/N 0102-014-6601

UNCLASSIFIED

SECURITY CLASSIFICATION OF THIS PAGE (When Data Entered)

ABSTRACT

Plasma wave measurements using instruments on the IMP 6 and Hawkeye 1 satellites are utilized in a study of very intense electrostatic waves near the upper hybrid resonance frequency in the region just outside the plasmapause. These intense plasma wave events have electric field strengths of ~ 1 to 20 mV m^{-1} and are among the most intense waves seen in the earth's magnetosphere. Detailed studies of more than 140 of these intense electrostatic disturbances reveal that the events occur at all local times and at magnetic latitudes varying from the equator to as high as 50°. The polarization of these waves is such that the wave electric field vector is oriented perpendicular to the geomagnetic field. In most cases the center frequency of the intense waves appears to correspond to an $(n + 1/2)f_g$ harmonic near the upper hybrid resonance frequency.

A survey of plasma measurements made simultaneously using the Hawkeye 1 LEPEDEA shows that the occurrence of the intense electrostatic waves is not strongly controlled by the intensities of ~ 1 to 20 keV electrons, but that specific details of the hot electron distribution function are directly related to the wave turbulence. All events at magnetic latitudes less than about 10° show strong pitch angle anisotropy with the greatest intensities at $\alpha \approx 90°$. The hot distribution function, $f(v_\perp, v_\parallel)$, is described

for a few events showing two sources of free energy; a temperature anisotropy and a loss-cone distribution. One event shown suggests that a bump-on-tail in $v_\perp$ may also contribute free energy in some cases.

A possible mechanism for producing intense waves near the upper hybrid resonance frequency is suggested which draws upon current theories applied to the generation of $(n + 1/2)f_g$ bands. Evidence is given which suggests the intense electrostatic waves may be a source of nonthermal continuum radiation.

INTRODUCTION

This paper describes very intense electrostatic waves occurring just beyond the plasmapause at frequencies close to the local upper hybrid resonance frequency, f_{UHR}. The importance of these waves is accentuated by their large amplitudes, ranging from about 1 to 20 mV m^{-1}, making them some of the most intense waves detected within the magnetosphere of the earth.

Weaker bands of electrostatic waves in the magnetosphere near f_{UHR} have been studied previously. Gurnett and Shaw [1973], Mosier et al. [1973], Shaw and Gurnett [1975], and Hubbard and Birmingham [1978a,b] have discussed bands of electrostatic emission at or just outside the plasmapause. The frequencies of those bands varied directly with upper hybrid resonance frequency over a region extending from just inside the plasmapause, across the abrupt decrease in plasma density (frequency) at the plasmapause, and into the outer magnetosphere. This signature appeared in about two-thirds of the IMP 6 plasmapause crossings. The band near f_{UHR} at the plasmapause was identified as upper hybrid resonance noise (in the terminology of Gurnett and Shaw [1973]). Outside the plasmapause diffuse electrostatic bands and narrow-band electrostatic noise were identified with emission frequencies between harmonics of the electron gyrofrequency, f_g^- [Shaw and Gurnett, 1975].

The intense electrostatic waves reported in this paper are probably related to one or more of the bands discussed by Shaw and Gurnett [1975]. In fact, the intense bands studied here often appear to be very intense upper hybrid resonance noise. It is important to note that Shaw and Gurnett have suggested the possibility of two distinct populations of events distinguishable by intensity. Evidence for the two populations is presented in their Figure 7 by means of a histogram for the number of electrostatic noise bands at 31.1 kHz as a function of peak electric field spectral density. The primary peak in occurrence frequency is located at about 10^{-15} V^2 m^{-2} Hz^{-1}, with a small secondary peak located near 10^{-9} V^2 m^{-2} Hz^{-1}. The intensities of the bands contributing to the secondary peak are similar to the intensities of the waves reported in this paper.

In this paper we treat only the most intense electrostatic waves found near the plasmapause and consider them to represent a class of waves unique from the low intensity bands discussed by Shaw and Gurnett [1975], even though the very intense waves are similar in many respects to the lower amplitude waves. We seek to understand why these waves are so much more intense. Since the initial report by Shaw and Gurnett [1975] which alluded to the existence of intense electrostatic waves near f_{UHR}, there have been other reports of such waves in the literature. Gurnett [1975] shows a very intense electrostatic wave event in his Figure 13 which appears to be associated with nonthermal continuum radiation. Using the passive plasma wave receiver on board GEOS 1

Christiansen et al. [1978] detected a similar intense band near f_p^- at about 6.5 R_E and suggested it might be an example of coherent electron cyclotron harmonic emission. Most recently Gurnett et al. [1978] have shown a very intense band (~ 7 mV m^{-1}) just outside the plasmapause near the lower frequency cutoff of the nonthermal continuum radiation detected with the plasma wave receiver on ISEE 1. Until now, no concerted effort has been made to study the occurrence and origin of these waves in a systematic manner. It is the purpose of this paper to [illegible]re the intense electrostatic waves beyond the plasmapause near f_{UHR} in detail. We shall describe the spectral characteristics, polarization, and the region of occurrence of the waves as well as the association of these electrostatic waves with other wave modes in the magnetosphere such as odd, half-harmonics of the electron gyrofrequency and nonthermal continuum radiation.

The plasma wave receivers on board the IMP 6 and Hawkeye 1 satellites are well suited to study electrostatic waves in the magnetosphere. The satellites were placed in highly eccentric orbits with greatly different initial inclinations of 89.8° and 28.7° (for Hawkeye 1 and IMP 6, respectively), hence, large portions of the magnetosphere have been sampled. (See Figure 1 of Gurnett and Frank [1977] for an illustration of the portions of the magnetosphere sampled by Hawkeye 1 and IMP 6.) Each plasma wave receiver was designed to sample the broad frequency range occupied by characteristic frequencies of magnetospheric plasma. The plasma wave sensors and receivers on board IMP 6 are described by Gurnett and Shaw [1973] and the Hawkeye 1 plasma wave receiver is described by Kurth et al. [1975].

The interaction of the intense waves with magnetospheric plasma is important to the understanding of the wave generation mechanism. In support of this study of intense electrostatic waves we shall present the results of a survey of the plasmas within regions of the intense wave turbulence. Early observations of the plasma in the region just outside the plasmapause are given by Schield and Frank [1970] and DeForest and McIlwain [1971]. These papers describe the earthward edge of the plasma sheet and the injection of hot plasma sheet electrons into the electron trough during magnetic substorms. Anderson [1976] has demonstrated a correlation between intense electrostatic waves above f_g^- and the injection of 1.2 keV electrons into the region just outside the nightside plasmapause. The present study is not meant to be a comprehensive study of the plasma just beyond the plasmapause, but rather is concerned with the comparison of these plasmas with observations of intense electrostatic waves near f_{UHR}.

Measurements of the intensities of electrons and positive ions over an energy range from about 50 eV to 40 keV have been gained with LEPEDEA plasma instrumentation on board the Hawkeye 1 spacecraft. The nearly rectangular field of view of the plasma analyzer is directed normal to the spacecraft spin axis, with angular dimension 30° parallel to the spin axis and 8° in the plane of rotation. A thin-windowed Geiger-Mueller tube is provided as part of the plasma instrument to determine the directional intensities of electrons and protons at energies $E \gtrsim 45$ keV and $\gtrsim 600$ keV, respectively. Instruments similar to the Hawkeye LEPEDEA have been flown on the IMP and INJUN satellites and are described in detail in Frank [1967].

II. DESCRIPTION OF INTENSE ELECTROSTATIC WAVES BEYOND THE PLASMAPAUSE

A. Spectral Properties

An example of the intense electrostatic wave events detected by IMP 6 and Hawkeye is shown in Figure 1 to illustrate the main characteristics of the waves. This illustration shows the average and peak electric field strengths sampled in the eight highest frequency spectrum analyzer channels of the IMP 6 plasma wave experiment for a two-hour interval on January 18, 1972. The solid black area for each channel has a vertical extent proportional to the logarithm of the electric field strength averaged over 5.3-sec. intervals. The dots represent the peak electric field strengths detected during each averaging interval. The event present in the 56.2-kHz channel at about 1950 UT and with a peak electric field strength of 4.0 mV m^{-1} is typical of the electrostatic wave events discussed in this report. The location of the plasmapause shown in Figure 1 is identified by observing several characteristic changes occurring nearly simultaneously in the plasma wave spectrum and spacecraft-related interference. (For a discussion of methods useful in determining plasmapause locations by means of various signatures in plasma wave data see Shaw and Gurnett [1975].) The dashed line labelled f_{UHR} in Figure 1 provides an estimate of the upper hybrid resonance frequency and serves only to illustrate the anticipated drop of f_{UHR} due to the abrupt decrease in density at the plasmapause. In this case, it is apparent that the intense wave event lies very close to the plasmapause.

A consistent feature of the electric field spectrum of the waves studied here is their narrow bandwidth. The spectrum for the event shown in Figure 1 is illustrated in Figure 2. Notice that the intense wave spectrum is very sharply peaked at 56.2 kHz, with responses in the adjoining channels due principally to filter overlaps in the spectrum analyzer. The bandwidth of the waves is typically less than about 10 percent of the center frequency. Some examples of the intense waves appear in high resolution spectrograms made from Hawkeye and IMP 6 wideband analog data. None of the high resolution spectrograms show any evidence for intense wave events near f_{UHR} having bandwidths greater than about 10 percent. Occasionally, other narrow spectral features are present at higher frequencies in conjunction with the band near f_{UHR}, and these will be discussed in the section on the identification of the wave mode.

The intensity of the electrostatic turbulence varies greatly as a function of time. The dots in Figure 1 show the sporadic nature of the waves. Variations of more than an order of magnitude in electric field strength are commonly detected on time scales of several minutes to a few seconds. The spectrum in Figure 2 illustrates the variation of intensity over short time intervals.

While the average electric field spectral density in this example is about 7×10^{-11} V^2 m^{-2} Hz^{-1}, the peak is about 3×10^{-9} V^2 m^{-2} Hz^{-1}. This represents a variation of a factor of about 7 in electric field strength in 5.3 seconds.

The intense waves near f_{UHR} usually include a weak magnetic component. Following the terminology of Shaw and Gurnett [1975], we have consistently referred to the waves as being electrostatic, but as can be seen in Figure 3, a small but measurable magnetic field component is present. The electric-to-magnetic field energy density ratio for this example is about 1600, while the ratio is usually equal to or greater than about 1000 for the other events detected with IMP 6. In some cases, no magnetic component is detectable. Because the electric-to-magnetic field energy density ratio is very large compared to that for electromagnetic waves in free space, we refer to these waves as electrostatic. It is important to mention that magnetic field data for the frequency range of interest are available only in the IMP 6 data. We have assumed that features visible in the Hawkeye data which are similar to IMP 6 events in their electric field characteristics also have similar magnetic field properties.

B. Regions of Occurrence

The initial isolation and characterization of the intense electrostatic waves discussed in this paper were achieved through a semi-automatic search of plasma wave data acquired with the IMP 6 and Hawkeye 1 satellites. Electrostatic bands near f_{UHR} are narrowband and fluctuate rapidly in intensity on time scales of seconds or less. A computer algorithm is used to select narrowband ($\Delta f/f \leq 10$ percent) events by seeking responses in a single channel which are stronger by a factor of at least 3 than the responses in adjacent channels. The algorithm also selects events which exhibit rapid fluctuations in intensity by requiring a peak-to-average electric field strength ratio greater than about 3. Finally, only those events with maximum electric field strength greater than about 1 mV m^{-1} are selected. Waves of lower intensity have been studied in detail elsewhere [Shaw and Gurnett, 1975].

Intense electrostatic waves at lower frequencies, e.g., near $3f_g^-/2$ have been studied extensively [Kennel et al., 1970; Fredricks and Scarf, 1973; Scarf et al., 1973]. Hence, in this paper we seek to extend the study of electrostatic waves in the magnetosphere to intense waves at frequencies usually much greater than f_g^-, i.e., f_p^- or f_{UHR}. While the electron plasma frequency may drop to as low as 500 Hz in portions of the magnetotail, f_p^- is usually greater than about 5 kHz for most regions of the magnetosphere. The range of magnetospheric gyrofrequencies beyond the plasmapause is about 500 Hz to 15 kHz. Hence, the search was conducted at IMP 6 analyzer center frequencies of 5.62, 10.0, 16.5, 31.1, 56.2 and 100 kHz. Two analyzer center frequencies of the Hawkeye plasma instrument were located at slightly different values of 13.3 and 17.8 kHz (versus the 10.0- and 16.5-kHz channels of IMP 6).

Once the list of possible events with narrow spectral structure and large, sporadic amplitudes is generated, the process of gaining specific information on individual events must proceed by hand. In addition to the intense electrostatic events of interest the list includes events for which (1) the waves are clearly electromagnetic, (2) the wave frequencies are well below f_p^-, and (3) the waves do not occur within the magnetosphere of the earth, such as electron plasma oscillations in the solar wind. The list is refined by hand to accomplish two goals. First, we eliminate events which are clearly not electrostatic waves near f_p^- or f_{UHR} in the magnetosphere and second, we attempt to classify and characterize the remaining events. The refining process relies heavily on the use of high resolution, frequency-time spectrograms which display the wideband analog data gained with each of the plasma wave instruments.

Through our search of over five and one-half years of IMP 6 and Hawkeye observations we have collected approximately 145 electrostatic events with intensities $\geqslant 1$ mV m^{-1}. The positions of these intense events are identified in Figure 4, with the figure organized to show four 6-hour segments of local time centered at magnetic noon, midnight, dusk, and dawn. Positions determined within each six-hour quadrant have been rotated (not projected) into the designated meridional plane (e.g., all local times from 2100 through 0300 are rotated into the midnight meridian). The points plotted in Figure 4 represent events detected in each of the six frequency channels from 5.62 kHz through 100 kHz.

It is apparent from Figure 4 that intense electrostatic waves near the f_{UHR} occur at all local times and over a wide range of latitudes. An examination of the local time distribution of the events on a finer scale than that of Figure 4 does not reveal significant preference for any local time. The limits of latitudinal coverage by the two satellites are indicated by dashed lines, with coverage within the limits not uniformly distributed. The apparent cutoffs in the occurrence of events near magnetic latitudes $\pm 50°$ may represent observational limits and not upper bounds for the phenomena. Orbital coverage is also greatly reduced near the magnetic equator due to the relatively large inclinations of the orbits relative to the magnetic equator. Because of this sampling bias greater numbers of intense events may lie close to the equator than are indicated by Figure 4. Kennel *et al.* [1970] and Fredricks and Scarf [1973] have reported increased occurrence frequencies for intense $3f_g^-/2$ and $(n + 1/2)f_g^-$ bands near the equator.

With a sample of only 145 events it is difficult to perform detailed statistical studies. We believe it is significant, however, that from the more than five and one-half years of observations comprising on the order of 1500 plasmapause crossings, the intense waves were observed during only about 10% of the crossings. This implies either that the intense waves are not present most of the time, or that they are confined to localized regions near the plasmapause surface which cover only about 10% of the area normally traversed by Hawkeye and IMP 6. The frequency of occurrence of events at latitudes within ± 10° of the magnetic equator is significantly higher than 10%. On the order of one of every three passes of Hawkeye or IMP 6 through the region within 10° of the magnetic equator for $3 \leq R \leq 8\ R_E$ reveal intense waves near f_{UHR}.

On a few occasions intense electrostatic wave events have been detected in nearly the same region of the magnetosphere and at the same frequency on two consecutive orbits. Some of the event-pairs display striking quantitative similarities suggesting these are not just random, unrelated occurrences. The observation of similar events on successive orbits may imply that the lifetime of these intense wave events can be as long as two to four days (the orbital periods of Hawkeye 1 and IMP 6, respectively). Evidently, the conditions necessary for the generation of the intense waves are present for periods of time of several hours to a few days and this lifetime could possibly give clues as to the origin of the waves. A reasonable explanation of event lifetimes on the order of a few days is that the intense electrostatic events are related to magnetic storms. A relationship with storms might also explain the infrequent occurrence of the events. However, a study of hourly D_{st} values at times when the intense wave activity was detected yielded a poor correlation between the wave events and magnetic storms. Only about half of the events showed any association with storms. The values of K_p during the intense wave events were also analyzed. The distribution of K_p during the events is not significantly different from the K_p distribution for all times, hence, no strong association with magnetic activity appears to exist.

A strong correlation between wave frequencies and the radial distance of intense wave events is observed. This trend is illustrated in Figure 5 by plotting the number of events detected in each frequency channel as a function of radial distance from the earth. The progressive decrease in wave frequencies of the events with increasing radial distances is unmistakable. We have observed approximately 15 events for which the band of emission was present for an interval of time sufficient for the frequency to drift from one channel to the next. In all of these events, the drift was to lower frequencies as a function of increasing radial distance. This relationship is almost certainly due to a close physical connection between the frequencies of these intense bands of electrostatic waves and characteristic frequencies of the local plasma. In this region of the magnetosphere, both the electron plasma frequency and the electron gyrofrequency show monotone decreases with increasing radial distance. It follows that the upper hybrid resonance frequency decreases at the same time (or over the same region of space). In general, the intense electrostatic wave events are observed at frequencies above, and often several times greater than f_g^-. Therefore, we feel confident that the instability is most closely related to either f_p^- or f_{UHR}. Evidence is presented in the next section which indicates the intense electrostatic turbulence is directly related to f_{UHR}. The electron gyrofrequency may remain an important parameter through the $(n + 1/2)f_g^-$ bands. This idea shall be developed further in the next section.

Other parameters which characterize the intense electrostatic waves detected near f_{UHR} include the duration (or spatial extent) and the distance from the plasmapause. These parameters are observed to vary greatly in magnitude from event to event with the events illustrated in Figures 1 and 3 demonstrating some of these variations. For example, notice in Figure 3 that the intense waves clearly lie outside the plasmapause, with the center of the event located nearly 0.5 R_E beyond the plasmapause. In contrast, the event shown in Figure 1 lies just at the plasmapause. Typically, the events range from being just at the plasmapause to a few R_E outside. The average distance is about 1.3 R_E from the plasmapause. The typical event lasts about 5 to 15 minutes which translates into an average radial extent of about 0.35 R_E. There is wide variability in the radial extent of the events, ranging from less than 0.1 R_E to more than 1 R_E.

C. Identification of the Wave Mode

By analyzing the polarization of the intense waves and studying other wave modes present in the vicinity of the intense events we can gain information necessary to identify the wave mode of the intense waves. For example, consider the plasma wave observations gained with Hawkeye 1 on January 31, 1976 during an outbound traversal of the magnetosphere near 10 hours magnetic local time. A portion of the observations are presented in Figures 6a and again in 6b to demonstrate the presence of intense waves with peak electric field strengths > 10 mV m^{-1} in the 31.1-kHz channel between 1840 and 1853 UT. Figure 6a is divided into three regions according to wave polarization. The polarization is determined by analyzing the electric field amplitude as a function of the angle between the electric dipole antenna and the geomagnetic field, $\vec{B}_o$. The shaded regions indicate where the polarization of the waves present is such that the electric field of the wave is nearly parallel to $\vec{B}_o$. Regions of the figure lacking shading or hatching indicate where the polarization of waves present is such that the electric field is nearly perpendicular to $\vec{B}_o$. The hatching indicates that region below f_g^- consisting of whistler-mode waves which are not of primary interest here. Superimposed on the presentation of Figure 6b is a solid line to specify the electron gyrofrequency and dashed lines for the first four $(n + 1/2)f_g^-$ harmonics. The magnetic field intensities required to calculate f_g^- were obtained by means of the onboard magnetometer, and were provided by J. A. Van Allen [personal communication, 1978]. Since the spacing of the eight frequency channels is approximately logarithmic, the ordinate of this figure may be defined as a frequency scale with the baseline of each channel marking the position of the center frequency of that channel.

As shown in Figure 6a the polarization of the intense electrostatic turbulence at 31.1 kHz is such that the wave electric field is perpendicular to the geomagnetic field, $\vec{B}_o$. The perpendicular polarization of these waves provides the best evidence that the waves are most closely related to f_{UHR} and not f_p^-. There are no modes at f_p^- which have perpendicular polarizations, whereas the modes at f_{UHR} are all polarized perpendicular to $\vec{B}_o$ [Shaw and Gurnett, 1978]. Other events have been analyzed for polarization with each one showing a perpendicular rather than parallel polarization.

Figure 6b shows that the intense electrostatic waves in the 31.1-kHz channel lie directly at the $7f_g^-/2$ harmonic. Diffuse electrostatic waves in the 23.7- and 17.8-kHz channels also align well with the $7f_g^-/2$ band, but these are very weak. From Figure 6b one can visualize a continuous band at $7f_g^-/2$ which suddenly intensifies near 1845 UT. Most of the events studied may be interpreted as intensifications of one of the $(n + 1/2)f_g^-$ bands.

There is sufficient information available in Figure 6a,b to identify the frequency of the intensification of the $7f_g^-/2$ band as f_{UHR}. The waves in the shaded region of Figure 6a, consisting of low amplitude waves with $\vec{E}\|\vec{B}_o$, are almost certainly continuum radiation propagating mainly in the (L, O) mode (in the convention of Stix [1962]). The intense wave event is located very close to the lower frequency cutoff of the continuum radiation which must be f_p^-. Since the intense waves are at about 3.5 f_g^-, $f_p^- \approx f_{UHR}$, and as discussed above, the perpendicular polarization of the intense wave turbulence unambiguously identifies f_{UHR} as the characteristic frequency important in the instability. Therefore, the event shown in Figure 6a,b is an intensification of the $7f_g^-/2$ band at f_{UHR}.

There exist many other examples of intense wave events occurring at f_{UHR} when $f_{UHR} \approx (n + 1/2)f_g^-$. Figure 7 displays IMP 6 wide-band data in a mode which cycles through bandwidths of 0.65 to 10 kHz 11 to 19 and finally 21 to 29 kHz (not shown) while alternately switching between a magnetic loop antenna and an electric dipole antenna. During this time interval the electron gyrofrequency is about 1.9 kHz (based on IMP 6 measurements of the magnetic field obtained from the National Space Science Data Center, N. F. Ness and D. H. Fairfield, principal investigators) and electrostatic bands near $3f_g^-/2$ and $5f_g^-/2$ are clearly seen. Continuum radiation is detected in the magnetic spectrogram with a lower cutoff at 15 kHz. (Due to the AGC characteristics of the receiver, the gain of the receiver is set much higher in the magnetic portion of the cycle allowing the detection of the weak continuum radiation. The presence of the intense band at about 15.2 kHz in the electric portion of the cycle sets the gain to a low value, hence, the continuum radiation can no longer be detected.) The intense electrostatic band at about 15.2 kHz is at a frequency very close to $15f_g^-/2$. Notice that the emissions near 15 kHz are separated by a frequency very close to f_g^-. Also, if the lower frequency of the continuum radiation is f_p^-, then f_{UHR} is very nearly 15.2 kHz. The significance of $f_{UHR} \approx (n + 1/2)f_g^-$ for the intense wave events will be addressed in the discussion section.

The question which remains concerning the event in Figure 6 is the explanation of the apparent spread in frequency of the intense event. It appears that the emissions occupy a very broad band of frequencies extending at least from 13.3 kHz to 178 kHz. The responses of all but the two channels adjacent to the 31.1-kHz channel are too great to be attributed to a single, narrowband signal at 31.1 kHz. There are three possible explanations for the responses in the other channels: (1) the event is broadband, (2) there is distortion due to receiver saturation, or (3) the event consists of multiple bands. From our survey of the high resolution spectrograms we can eliminate the possibility of the event being broadband since no evidence for broadband events has been seen. Without high resolution spectrograms for this specific example, however, the other two possibilities must remain.

We should point out that evidence of multiple-banded events has been found in at least one example from observations with the Hawkeye instrument. In that case a band was detected above f_{UHR} which was definitely not the result of harmonic distortion. The spacing of the two bands was not related to f_g^-, hence the upper band could not be identified as an $(n + 1/2)f_g^-$ harmonic. Specific examples of multiple-banded events which are most likely due to harmonic distortion can also be found in the wideband analog data.

III. SIMULTANEOUS OBSERVATIONS OF HOT PLASMAS

A. Survey of Properties

For the 50 intense electrostatic wave events detected with the Hawkeye plasma wave instrument, 47 simultaneous measurements of hot plasma distributions are available from the companion LEPEDEA plasma analyzer. An initial survey of these plasma observations was accomplished by means of energy-time (E-t) spectrograms of the analyzer responses, examples of which are displayed in Plates 1 and 2. The proton observations will not be discussed as wave frequencies of interest are sufficiently high so that wave-particle interactions with the protons are considered to be negligible. At energies less than several hundred electron volts the electron measurements may be aliased by spacecraft charging within the range $4 \leqslant L \leqslant 8$ [Gurnett and Frank, 1976]. Therefore, we have restricted the survey to energies $E \geqslant 900$ eV (electron velocities $\geqslant 1.8 \times 10^9$ cm sec^{-1}). Such a concentration on the hotter-component of the electron spectrum is suppoerted by the work of Lyons [1974], in which it was demonstrated that the greater the wave energy of electrostatic waves at $f > f_g^-$ the greater the energies of the electrons diffused by these waves.

Each plate comprises three panels for the presentation of LEPEDEA plasma measurements with a common time base displayed along the ordinate of each panel. Identification of spatial position is provided at 10-minute intervals by the inclusion of geocentric radial distance, in R_E, invariant latitude, in degrees, and magnetic local time, in hours. The formats of the upper and middle panels are identical, with each color spectrogram accompanied by a plot of the pitch angles of the particles detected. Numerical values on the abscissas of the spectrograms are approximately equal to the logarithm of energy, from 50 eV to ~ 20 keV. Pitch angles are displayed linearly over the range 0° - 180°. The systematic samplings in pitch angles with a period of ~ 3 minutes arises from similar periods for the spacecraft rotation rate and the analyzer repetition rate for the individual energy scans. The color bar is calibrated in units of the logarithm of the instrument responses, counts sec^{-1}. We will not be concerned with observations presented in the bottom panel.

In general it can be stated that measurable intensities of electrons at energies $E \geq 900$ eV have been detected for all except one of the intense electrostatic wave events for which simultaneous observations are available. The durations of measurable electron intensities were generally greater (but not less) than the typical 10-minute durations for wave events, however, and the relative locations of the wave events within the regions in which plasma was detected appeared to vary.

For 26 percent of the cases studied the spatial (temporal) correlations are very good between the positions of the most intense electron intensities and wave intensities. Such a case is illustrated with the aid of Plate 1 and the display of wave intensities in Figure Figure 8. The greatest wave intensites are found in the 17.8-kHz channel during the time interval 2258 - 2305 UT, and are preceded by a ~ 10-minute period of less intense emissions principally at the lower frequencies. The time interval of greatest electron intensities corresponds almost exactly with that for the most intense wave activity. Other notable features of the plasma observations are: (1) a weak pitch-angle anisotropy early in the one-hour period which diminishes in amplitude as the range of pitch angles scanned decreases, (2) gradual increases in mean energy and intensities in the early period prior to ~ 2258 UT, corresponding to the interval of relatively weak wave emissions, and (3) an abrupt decrease in intensities at ~ 2305 UT. This series of observations was gained at a comparatively high magnetic latitude of 54°. The narrow intensity peaks of large amplitude which appear to 'walk' across the electron spectrogram in Plate 1 represent analyzer responses to scattered solar Lyman-α radiation.

For the 74 percent of the events in which such a striking correlation is not present one observes typically a much broader region of plasma-sheet-like plasmas than that illustrated in Plate 1, with the more spatially confined wave event located within. The spectrograms do not typically reveal noticeable changes in the signature of the electron intensities when entering into and/or exiting from a period (or region) of intense wave activity, though striking examples do exist. Of the events at magnetic latitudes greater than 20° virtually all of those events showing poor correlations between intense wave events and obvious plasma signatures lie at magnetic local times between about 4 hours and 20 hours. Events showing good correlations at latitudes above 20° lie between about 20 hours and 4 hours magnetic local time. Notice that the event with good temporal correlation shown in Figure 8 and Plate 1 is an apparent exception to this local time trend. Local time does not appear to affect the wave-plasma correlation for events near the magnetic equator. Thus it appears that the presence of measurable intensities of $\gtrsim$ 900-eV electrons is necessary, but it need not be a sufficient condition for the presence of intense electrostatic wave activity.

For 30 percent of the events studied the magnetic latitude of the spacecraft was sufficiently low and the spin axis appropriately directed to enable the plasma analyzer to sample a wide range of pitch angles. In all of these 14 events the electron intensities at α = 90° and relative minima at 0° and 180°. Typical of these cases are the observations summarized in the spectrogram of Plate 2, where anisotropic electron intensities were detected near the magnetic equator for a period of ~ 25 minutes between 2155 and ~ 2220 UT. Telemetry was interrupted in the earlier interval 2145 - 2155 UT, but observations prior to signal loss illustrate the presence of measureable intensities over the more limited pitch-angle range then being scanned. After ~ 2220 UT the intensities of more energetic electrons approached threshold levels. The enhanced intensities of lower-energy electrons detected just equatorward of the plasmapause (crossed at ~ 2210 UT) are the subject of other work and will not be discussed.

It is in the narrow time interval 2204 - 2207 UT that a significant departure is noted from the average in energetic electron intensities over the 25-minute interval of interest. The intensities of electrons with energies $E \simeq$ 1-2 keV increase by a factor of ~ 10 at pitch angles $\alpha \simeq 90°$, thereby increasing the magnitude of the previously existing anisotropy. In the 2204 - 2207 UT interval the ratio in intensities between $\alpha = 90°$ and 70° is ~ 10. Plasma wave observations shown in Figure 9 demonstrate the presence in this time interval of an intense wave event with maximum electric field strengths of ~ 6×10^{-4} V m^{-1} at 100 kHz.

In summary, the intensities of $\gtrsim$ 900-eV electrons in the vicinity of intense electrostatic wave events and near the magnetic equator appear to be anisotropically peaked at $\alpha = 90°$. For several of the events noticeable increases in the intensities at $\alpha = 90°$ can be closely associated with the presence of intense electrostatic wave activity. In these cases the anisotropies in electron intensities can be as great as a factor of ~ 10 at some energies only 15° - 20° away from $\alpha = 90°$.

Typical electron intensities at 10 keV, for example, ranged from ~ 2×10^3 to ~ 2×10^4 $(cm^2 - sec - sr - eV)^{-1}$ at $\alpha \simeq 90°$ and low magnetic latit... The absence in one case of measurable electron intensities ... t magnetic ... titudes of $\sim 20°$ during a wave event is consistent with the presence of a highly anisotropic distribution with intensities ... $\sim 10^3$ $(cm^2 - sec - sr - eV)^{-1}$ at equatorial pitch angle $\alpha_o = 90°$ and energies of ~ 10 keV.

B. Electron Distribution Functions

In search of free energy sources to drive intense electrostatic wave growth, the Hawkeye data were surveyed to isolate those intense events for which simultaneous wave and plasma observations were available within several degrees of the magnetic equator. Four cases qualified for analysis based upon the need of adequate analyzer responses at pitch angles as small as $\alpha = 30°$. Sample densities were improved by assuming that the electron intensities were hemispherically and gyrotropically symmetric. Electron distribution functions $f(v_\perp, v_\parallel)$ were then constructed for an energy range extending from ~ 1 to ~ 38 keV.

Several sources of free energy have been suggested which are based upon velocity anisotropies in the hot electron component of distribution functions. The signature of one such source is the appearance of a positive slope in the perpendicular velocity component, $\partial f(v_\perp, v_\parallel)/\partial v_\perp > 0$, at fixed $v_\parallel$. Variations on the classical bump-on-tail distribution for the component $f_\perp(v_\perp)$ have been studied, for example, by Fredricks [1971] and Young et al. [1973]. The criterion is also satisfied at small $v_\perp$ in the hot component by means of loss-cone distributions for which contours of $f(v_\perp, v_\parallel)$ = constant become indented about the $v_\parallel$ axis [e.g, Ashour-Abdalla and Kennel, 1978a]. A second signature which apparently need not satisfy the above criterion is that of a small temperature anisotropy for which $T_\perp/T_\parallel > 1$ [Ashour-Abdalla and Cowley, 1974]. These two signatures have been observed in distribution functions obtained with the LEPEDEA plasma analyzer.

The first event to be examined is from April 5, 1977, during the outbound portion of orbit 487 and demonstrates the presence of a loss-cone distribution at the magnetic equator. The time-history of the wave event is displayed in Figure 10, where it can be seen that wave activity was intense between ~ 0415 UT and ~ 0438 UT, with peak activity recorded at ~ 0431 UT in the 17.8-kHz channel. The intensities of ⩾ 1-keV electrons (not illustrated) increased significantly simultaneously with the onset of wave activity, and remained at large flux levels until after 0500 UT. No significant charges are visible in the E-t spectrogram for this event at ~ 0438 UT when the wave intensities decreased sharply. The electron velocity distribution function presented in Figure 11 results from observations in the interval 0429 - 0433 UT (centered on peak wave activity). It possesses a well-defined loss cone at pitch angles $\alpha \leqslant 25°$ with $\partial f/\partial v_\perp > 0$ for $v_\parallel > 2 \times 10^9$ cm sec^{-1}. The distribution function is approximately Maxwellian at each pitch angle for $f \leqslant 10^{-31}$ cm^{-6} sec^3, but the temperature at $\alpha = 15°$ is a factor of ~ 2 less than that at $\alpha = 80°$. The temperature decreases uniformly with pitch angle in the intermediate angles.

The dashed line traversing contours of constant phase-space density at low values of $v_{\perp}$ represents the locations at which the analyzer response equals 100 counts sec^{-1}, and serves to delineate the portion of the distribution function at lower $v_{\perp}$ for which the counting statistics of the digital-to-analog rate meter require increasing attention. Contours are not displayed for average responses less than 50 counts sec^{-1}.

The second of the four events analyzed has yielded a distribution function displaying features qualitatively similar to those presented in Figure 11. The loss cone is less-clearly defined, but the temperature anisotropy for Maxwellian fits at pitch angles $\alpha = 90°$ and $15°$ is nearly equal to 2. And again, the temperature decreases smoothly at the intermediate values of α.

The third event analyzed provides an example of an electron distribution function which exhibits a loss-cone distribution but no significant temperature anisotropy. The time history of the wave event detailed in Figure 12 indicates that two brief wave bursts were recorded in the interval 2342 - 2350 UT, and that peak wave intensities of ~ 0.6 mV m^{-1} were detected in the 100-kHz channel. An E-t spectrogram for this period shows that the brief wave events occurred within a larger time interval of ~ 30 minutes duration during which highly anisotropic and energetic electron intensities were detected. No corresponding changes are noted at the times of the wave events. The distribution function of Figure 13 was constructed from observations acquired in the interval

2346 - 2350 UT during which the second of the two wave events took place. The loss cone is clearly present at $v_{\parallel} \geqslant 2 \times 10^9$ cm sec^{-1}. The distribution may be approximated by a Maxwellian at fixed pitch angles and at energies $E \geqslant 10$ keV, but it is less convincing than for the first two events discussed. No significant temperature anisotropy exists between pitch angles $\alpha = 85°$ and $25°$. The distribution is is more strongly peaked at large pitch angles $\alpha \geqslant 75°$ than for the first two cases.

The fourth distribution function has been obtained from plasma observations presented previously in Plate 2 and discussed in conjunction with the wave event of Figure 9. The distribution function presented in Figure 14 details the state of the energetic electron population in the interval 2205 - 2207 UT for which peak wave activity was recorded. The E-t spectrogram for the event displays a brief period of enhanced electron intensities centered on the time of the maximum wave intensities. No conclusions can be drawn about the form of the distribution function at pitch angles $\alpha \leqslant 30°$ as average analyzer responses are < 50 counts sec^{-1}. The distribution is strongly peaked at large pitch angles. The gradient $\partial f/\partial v_{\perp}$ is sufficiently small at $\alpha \simeq 90°$ and velocities $v_{\perp} \simeq$ 6-to-10 $\times 10^9$ cm sec^{-1} to suggest the presence of a narrow region of zero slope at the least and a small bump-on-tail distribution at best. The latter distribution could not be resolved with the Hawkeye analyzer at those energies.

The distribution functions presented have been computed from intensity measurements gained with a plasma analyzer of finite field of view which is rectangular and measures 8° x 30°. For analyzer orientations normal to $\vec{B}$ the range of pitch angles sampled was confined to $\alpha = 90° \pm 4°$. This presents no concern. However, when oriented parallel to $\vec{B}$ the 15° half-angle permits the sampling of pitch angles $\alpha = 0°$ to 15° and can result in an overestimate of phase-space densities at the smallest angles. A quantitative demonstration of the consequences of a finite field of view has been prepared by choosing an analytic representation for a loss-cone distribution and calculating the distribution function which would be deduced from measurements with an analyzer of field of view 8° x 30°. Contours of constant $f(v_\perp, v_\parallel)$ are presented in Figure 15 as solid lines for a subtracted bi-Maxwellian distribution [Ashour-Abdalla and Kennel, 1978a]. The free parameters selected are $n_h = 0.125$ cm^{-3}, $E_\perp = 10$ keV, $E_\parallel = 3$ keV, $\beta = 0.9$ and $\Delta = 0$. (β and Δ are parameters quantifying the width and depth of the loss-cone distribution as defined by Ashour-Abdalla and Kennel [1978a].) A strong loss cone is developed at pitch angles $\alpha \leqslant 25°$ with a large anisotropy present at greater angles. Corresponding computed instrument responses are shown by dashed lines which differ from the actual contours only at pitch angles $\alpha \leqslant 25°$. It can be seen that the largest overestimates in this example appear for angles $\alpha \leqslant 15°$.

In summary, electron distribution functions studied reveal the presence of temperature anisotropies and/or loss-cone depletions which are believed to represent sources of free energy for the growth of electrostatic waves. The depths of the loss cones at the smallest pitch angles sampled may have been underestimated due to the finite field of view of the plasma analyzer.

IV. DISCUSSION

A. Possible Mechanisms For Generating Intense Electrostatic Waves Near f_{UHR}

The Harris dispersion relation [Harris, 1959] undoubtedly includes the instability responsible for the generation of the intense electrostatic turbulence discussed herein, but it is not a simple task to determine the way in which several parameters act together to produce the highly unstable mode reported in this paper. Shaw and Gurnett [1975] discuss the application of the Harris dispersion relation to the electrostatic bands reported in that paper, including the diffuse electrostatic bands and narrowband electrostatic noise. The UHR band similar to that reported by Mosier *et al.* [1973] and Gurnett and Shaw [1973] has been interpreted as Cerenkov noise from energetic particle fluxes by Gregory [1971]. Taylor and Shawhan [1974] calculate that sufficiently large electric fields are generated between the local plasma frequency and f_{UHR} by incoherent Cerenkov radiation from thermal electrons to explain the upper hybrid resonance band at the wave amplitudes treated by Gurnett and Shaw.

Waves at or near the $(n + 1/2)f_g^-$ harmonics have been reported by many, including Kennel *et al.* [1970], Fredricks and Scarf [1973], and Scarf *et al.* [1973] and have been studied theoretically most recently by Ashour-Abdalla and Kennel [1978a,b] and Hubbard and

Birmingham [1978a]. The latter three references show good qualitative agreement between growth rate calculations and the characteristics of $(n + 1/2)f_g^-$ waves. Ashour-Abdalla and Kennel [1978a] demonstrate that a large number of plasma parameters control the instabilities. For example, the cold electron temperature controls the spatial amplification of the waves while the cold-to-hot electron density ratio and the cold upper hybrid frequency control which bands are unstable. The underlying requirement for instability, however, is that the electron velocity distribution must have a region of positive slope with respect to the perpendicular velocity component, $v_\perp$.

All of the above work in the theory of electrostatic instabilities in the magnetosphere is important to the explanation of the intense electrostatic waves discussed in this paper. The code of Ashour-Abdalla and Kennel [1978b] can possibly be extended to the frequency range of these waves easily if the ratio of f_{UHR} (calculated using the cold electron number density) to f_g^- is not exceedingly high [Ashour-Abdalla, personal communication]. Even so, the plasma must be described by several parameters including the cold electron density and temperature as well as a description of the hot component, which, as shown in Section III, may take the form of a loss-cone distribution, and/or anisotropic distribution in temperature or possibly even a bump-on-tail distribution in $v_\perp$.

In light of the foregoing theoretical considerations we suggest that the fact that the intense electrostatic turbulence reported here is usually found when the band at f_{UHR} coincides with one of the $(n + 1/2)f_g^-$ bands is likely to account for the extreme intensity of the waves. While the intensifications of the band near f_{UHR} have not been treated directly in the theory, there is sufficient information available with which to formulate a scenario for explaining the intense waves. Hubbard and Birmingham [1978a] offer a classification scheme for electrostatic emissions between harmonics of f_g^- in the magnetosphere. Hubbard and Birmingham's "class 4" emissions include waves similar to the waves of primary importance in this paper in that the "class 4" waves occur between cyclotron harmonics near f_p^-.

Hubbard and Birmingham [1978a] predict wave growth near f_p^- if $f_p^- \approx f_{UHC}$ and if $n_c/n_h > 1$ where f_{UHC} is the upper hybrid resonance frequency calculated using the cold electron density and n_c and n_h are the cold and hot electron densities, respectively. In addition to waves near f_p^- ($\approx f_{UHC}$) the theory shows much weaker growth at higher and lower frequencies. The condition $n_c/n_h > 1$ is consistent with observations of the waves near f_{UHR} since f_{UHC} approaches f_{UHR} as n_c/n_h increases. In addition, the location of the intense waves near the plasmapause probably assures a relatively large n_c/n_h ratio.

Ashour-Abdalla and Kennel [1978b] provide a useful tool for applying the theory of $(n + 1/2)f_g^-$ emissions to waves near f_{UHR}. Figure 4 of that paper shows regions of nonconvective instability as a function of f_{UHC} and n_c/n_h. Nonconvective instability implies large growth rates since the waves do not propagate out of the region of amplification. The result of the study of regions of nonconvective instability is that for a wide range of n_c/n_h nonconvective growth will occur only at the $(n + 1/2)f_g^-$ band closest to f_{UHC}. Typically, T_c/T_h, the ratio of the cold-to-hot electron temperatures, must be less than about 5×10^{-2}, and $1.5 \leqslant n_c/n_h \leqslant 4$ for $f_{UHR} \leqslant 4f_g^-$.

The scenario, then, is that a low intensity band near f_{UHR} may commonly be observed at or beyond the plasmapause as reported by Gurnett and Shaw [1973] and Shaw and Gurnett [1975]. The low intensity UHR band may be the result of incoherent Cerenkov radiation [Taylor and Shawhan, 1974]. Then, under the proper plasma conditions, including the existence of a free energy source in the electron distribution function, nonconvective growth may set in for frequencies, f_w, such that $f_w \approx f_{UHR} \approx (n + 1/2)f_g^-$, assuming $n_c/n_h \geqslant 1.5$. The resulting waves will have $k_\perp \gg k_\parallel$ where $k_\perp$ and $k_\parallel$ are the perpendicular and parallel wave numbers, respectively. Hence, for electrostatic waves, the wave electric field is nearly perpendicular to $\vec{B}_o$. A fundamental requirement for the cyclotron instability is the presence of a positive slope in the perpendicular electron distribution function or a temperature anisotropy. Furthermore, the cold electron density and temperature play important roles in determining at which frequencies the instability grows and how rapidly. The study of the Hawkeye plasma data does not treat the cold electron distribution but provides several possibilities for free energy sources to drive the waves. It is significant that the hot distribution function of Ashour-Abdalla and Kennel [1978a] may be readily fit to the measured distribution functions shown in Section III. For example, at the larger velocities the model distribution function illustrated in Figure 15 displays qualitative features similar to the actual $f(v_\perp, v_\parallel)$ contours of Figures 11 and 13. Even though the entire distribution function remains unmeasured, the form of the loss-cone free energy source indicates that the theories of Ashour-Abdalla [1978a,b] and Hubbard and Birmingham [1978a] are based on reasonable model distribution functions. Obviously, the next steps in the study of this instability are to carry plasma measurements to lower energies, for example, with the ISEE Quadrispherical LEPEDEAs [Frank et al., 1978] and to more closely tune the model distribution functions utilized in the theoretical work to direct observations.

B. Intense Electrostatic Waves as a Source of Nonthermal Continuum Radiation

An issue of significant importance is whether or not these intense electrostatic waves are related to the generation of a portion of the earth's radio spectrum. It is reasonable to examine these regions of strong electrostatic waves in connection with the generation of the nonthermal continuum radiation. Gurnett [1975] reported the generation region to be a broad region outside the plasmapause at radial distances between 4.0 and 8.0 R_E and between about 0400 and 1400 hours local time. While this study reveals the intense electrostatic events at all local times, the radial distance range just outside the plasmapause is very similar to that found for the intense electrostatic waves. A significant relation between these intense electrostatic waves and the generation of continuum radiation is found in Gurnett and Frank [1976] in which it is argued that continuum radiation appears to be correlated with intensities of 1 to 20 keV electrons in the region $4 \leq L \leq 8$, similar to the electrons apparently involved in the instability generating the waves near f_{UHR}.

There are several other reasons to expect these electrostatic waves may be connected with the nonthermal continuum. Gurnett shows a typical spectrum of the continuum radiation (see Figure 4 of Gurnett [1975]) which has a lower frequency cutoff of about 3 kHz defined by the local electron plasma frequency in the magnetospheric cavity in which the lower frequency portion of the radiation is trapped. The upper frequency limit of the feature in Gurnett's spectrum is about 200 kHz. This range in frequency is very similar to the frequencies of the intense electrostatic waves near f_{UHR} (c.f., Figure 5). In fact, a few events were seen in the 178-kHz channels of Hawkeye and IMP 6 but those channels were not included in the search because of the difficulty in distinguishing between the electrostatic waves and auroral kilometric radiation.

Perhaps the most striking evidence suggesting these intense waves are a source for the continuum radiation is shown in Figure 16. An example of an intense wave event is shown in the bottom panel at about 0712 UT centered at about 4.3 R_E from the earth. In the interval from about 0720 to 1145 UT continuum radiation is seen to decrease smoothly in amplitude, presumably as a function of some distance. The center panel is a plot of the power flux of continuum radiation as a function of the distance of the satellite from the earth. We assume that the power flux will decrease as the inverse square of the distance between the receiver and a simple, compact source. The dashed line represents a function with a geocentric radial distance dependence of R^{-2}. There is clearly no reason to believe the source for the continuum radiation is centered at the earth based on the center panel. The top panel is another plot of the power flux of the continuum radiation, but as a function of (R-R') where R is the position of the satellite and R' is the position of the intense wave region. We have assumed that the earth, the intense waves, and the satellite are collinear for this simple demonstration. The dashed line in the top panel of Figure 16 is a function which is proportional to $(R-R')^{-2}$. There is very good agreement between the assumed geometry and the data in this top panel. We have made no attempt to do a least squares fit or to adjust R' for a better fit. We seek only to demonstrate that the continuum radiation clearly appears to be radiating from a source near 4.3 R_E and that the source is fairly compact.

There are several examples similar to that shown in Figure 16 which strongly suggest the intense waves are a local source of non-thermal continuum radiation (see Gurnett's [1975] Figure 13). Another example of this effect is seen in the IMP 6 orbit 76 event shown in Figure 1. We must say, however, that most events do not display any direct relationship to continuum radiation. The event shown in Figure 8 shows little, if any, continuum radiation which could be related to the intense waves. It is not clear why some events appear to be generating continuum radiation and others do not. Two possible explanations are that either the wave-wave interaction converting electrostatic waves into the electromagnetic mode is sometimes very inefficient or non-existent or there is a propagation effect which dictates regions or directions in which the waves will not propagate. An example of the latter case might be a wave-wave interaction which yields waves strongly beamed in particular directions as defined by wave-vector selection rules for that interaction.

It is not the purpose of this paper to prove that the intense electrostatic waves reported here are solely responsible for the generation of the nonthermal continuum radiation. We have shown, however, that several features of the electrostatic waves make them a possible source of continuum radiation. The event shown in

Figure 16 strongly suggests that intense electrostatic waves are at least secondary sources of nonthermal continuum radiation, even if there are other mechanisms producing the bulk of the electromagnetic radiation.

V. CONCLUSIONS

We have described a class of very intense electrostatic waves located at or just outside the plasmapause near the upper hybrid resonance frequency. The waves at amplitudes from ~ 1 to 20 mV m^{-1} are only observable in about 10% of the plasmapause crossings made by the Hawkeye 1 and IMP 6 satellites, however, they are among the most intense plasma waves seen in the magnetosphere. The observable characteristics of the waves are:

1. The waves are often very intense, > 10 mV m^{-1}.
2. The waves are narrowband and fluctuate rapidly in intensity.
3. The waves are found at all local times in a magnetic latitude range from the equator to at least $\pm$ 50°.
4. The waves occur at or just outside the plasmapause and the higher frequency events are found generally at smaller radial distances, i.e., closer to the plasmapause.
5. The waves usually lie between harmonics of f_g^-.
6. The waves also lie near f_{UHR}.
7. The waves are polarized such that the wave electric field is perpendicular to the geomagnetic field.
8. There is a small magnetic field component to the waves in many cases, but the electric-to-magnetic field energy density ratio is always very large.

In addition, evidence is given which strongly suggests the wave events are at least secondary sources of nonthermal continuum radiation.

Plasma measurements taken simultaneously with the detection of the intense waves show only a fair correlation with intensities of electrons in the energy range from about 1 to 20 keV. However, all events detected at the magnetic equator when an ample range of pitch angles is sampled show evidence of pitch angle anisotropies in favor of $\alpha = 90°$. Measurements of the velocity distribution function for events detected at the magnetic equator reveal two sources of free energy; a loss-cone distribution, and a temperature anisotropy with $T_\perp/T_\parallel > 1$. There is a suggestion of a possible third source of free energy in the form of a bump-on-tail in $v_\perp$.

A possible explanation of the intense electrostatic waves near f_{UHR} may exist in the theory of multi-cyclotron emissions. The theory predicts large spatial growth rates in the $(n + 1/2)f_g^-$ band including f_{UHC} while growth rates at other frequencies are smaller. The theory is based on a loss-cone distribution function which is qualitatively supported by simultaneous plasma measurements.

ACKNOWLEDGEMENTS

The authors are grateful to Professor J. A. Van Allen for allowing liberal use of measurements from the magnetometer on board Hawkeye 1. We are indebted to Drs. N. F. Ness and D. H. Fairfield for magnetic field data from IMP 6 used in Figure 7. We would like to thank Dr. M. Ashour-Abdalla and Professor C. F. Kennel for a series of discussions which have proven to be of great value in this study.

The research at the University of Iowa was supported by the National Aeronautics and Space Administration through Contracts NAS1-13129, NAS5-11074, Grant NGL-16-001-043, and by the U. S. Office of Naval Research through Contract N000 14-76-C-0016.

REFERENCES

Anderson, R. R., Wave-particle interactions in the evening magnetosphere during geomagnetically disturbed periods, Ph. D. dissertation, Dept. of Physics and Astronomy, University of Iowa, Iowa City, Iowa, 1976.

Ashour-Abdalla, M., and S. W. H. Cowley, Wave-particle interactions near the geostationary orbit, in Magnetospheric Physics, edited by B. M. McCormac, D. Reidel, Dordrecht, Netherlands, 1974.

Ashour-Abdalla, M., and C. F. Kennel, Nonconvective and convective electron cyclotron harmonic instabilities, J. Geophys. Res., 83, 1531, 1978a.

Ashour-Abdalla, M., and C. F. Kennel, Multi-harmonic electron cyclotron instabilities, Geophys. Res. Lett., 5, 711, 1978b.

Christiansen, P., P. Gough, G. Martelli, J.-J. Block, N. Cornilleau, J. Etcheto, R. Gendrin, D. Jones, C. Béghin, and P. Décréau, Geos I: identification of natural magnetospheric emissions, Nature, 272, 682, 1978.

DeForest, S. E., and C. E. McIlwain, Plasma clouds in the magnetosphere, J. Geophys. Res., 76, 3587, 1971.

Frank, L. A. Initial observations of low-energy electrons in the earth's magnetosphere with OGO-3, J. Geophys. Res., 72, 185, 1967.

Frank, L. A., D. M. Yeager, H. D. Owens, K. L. Ackerson, and M. R. English, Quadrispherical LEPEDEAS for ISEE's-1 and -2 plasma measurements, Geoscience Electronics, GE-16, 221, 1978.

Fredricks, R. W., Plasma instability at $(n + 1/2)f_c$ and its relationship to some satellite observations, J. Geophys. Res., 76, 5344, 1971.

Fredricks, R. W., and F. L. Scarf, Recent studies of magnetospheric electric field emissions above the electron gyrofrequency, J. Geophys. Res., 78, 310, 1973.

Gregory, P. C., Satellite observations of magnetospheric radio noise 1. Emissions between the plasma and upper hybrid resonance frequencies, Planet. Space Sci., 19, 813, 1971.

Gurnett, D. A., The earth as a radio source: The nonthermal continuum, J. Geophys. Res., 80, 2751, 1975.

Gurnett, D. A., and L. A. Frank, Continuum radiation associated with low-energy electrons in the outer radiation zone, J. Geophys. Res., 81, 3875, 1976.

Gurnett, D. A., and L. A. Frank, A region of intense plasma wave turbulence on auroral field lines, J. Geophys. Res., 82, 1031, 1977.

Gurnett, D. A., R. R. Anderson, F. L. Scarf, R. W. Fredricks, and E. J. Smith, Initial results from the ISEE-1 and -2 plasma wave investigation, (submitted to Space Science Rev.), 1978.

Gurnett, D. A., and R. R. Shaw, Electromagnetic radiation trapped in the magnetosphere above the plasma frequency, J. Geophys. Res., 78, 8136, 1978.

Harris, E. G., Unstable plasma oscillations in a magnetic field, Phys. Rev. Lett., 2, 34, 1959.

Hubbard, R. F., and T. J. Birmingham, Electrostatic emissions between electron gyroharmonics in the outer magnetosphere, J. Geophys. Res., 83, 4837, 1978a.

Kennel, C. F., F. L. Scarf, R. W. Fredricks, J. H. McGehee, and F. V. Coroniti, VLF electric field observations in the magnetosphere, J. Geophys. Res., 75, 6136, 1970.

Kurth, W. S., M. M. Baumback, and D. A. Gurnett, Direction-finding measurements of auroral kilometric radiation, J. Geophys. Res., 80, 2764, 1975.

Lyons, L. R., Electron diffusion driven by magnetospheric electrostatic waves, J. Geophys. Res., 79, 575, 1974.

Mosier, S. R., M. L. Kaiser, and L. W. Brown, Observations of noise bands associated with the upper hybrid resonance by the IMP 6 radio astronomy experiment, J. Geophys. Res., 78, 1673, 1973.

Scarf, F. L., R. W. Fredricks, C. F. Kennel, and F. V. Coroniti, Satellite studies of magnetospheric substorms on August 15, 1968, J. Geophys. Res., 78, 3119, 1973.

Schield, M. A., and L. A. Frank, Electron observations between the inner edge of the plasma sheet and the plasmasphere, J. Geophys. Res., 75, 5401, 1970.

Shaw, R. R., and D. A. Gurnett, Electrostatic noise bands associated with the electron gyrofrequency and plasma frequency in the outer magnetosphere, J. Geophys. Res., 80, 4259, 1975.

Shaw, R. R., and D. A. Gurnett, The low-frequency cutoffs of non-thermal continuum radiation: Comments on 'source of terrestrial non-thermal radiation' by D. Jones, University of Iowa Research Report 78-14, 30 p., 1978.

Stix, T. H., The Theory of Plasma Waves, McGraw-Hill, New York, 1962.

Taylor, W. W. L., and S. D. Shawhan, A test for incoherent Cerenkov radiation for VLF hiss and other magnetospheric emissions, J. Geophys. Res., 79, 105, 1974.

Young, T. S., J. D. Callen, and J. E. McCune, High-frequency electrostatic waves in the magnetosphere, J. Geophys. Res., 78, 1082, 1973.

FIGURE CAPTIONS

Plate 1 — An energy-time spectrogram for LEPEDEA plasma observations in the period 2230 - 2330 UT on April 23, 1976. This spectrogram was obtained during the high latitude wave event shown in Figure 8. The time correlation of the electron intensities at about 1 keV with the intense electrostatic waves seen in Figure 8 is very good.

Plate 2 — An energy-time spectrogram for LEPEDEA plasma observations in the period 2140 - 2240 UT on August 15, 1975. This spectrogram was obtained at the magnetic equator during the intense electrostatic wave event shown in Figure 10. Note the highly anisotropic electron intensities at about 1 keV between 2200 and 2210 UT.

NOTE: Plates 1 and 2 will be published in color.

Figure 1 An example of intense electrostatic waves detected just at the plasmapause by the University of Iowa plasma wave instrument onboard the IMP 6 satellite. The solid black areas have a vertical extent proportional to the average electric field strength during 5.3 second averaging intervals. The dots indicate the peak electric field detected during the same interval.

Figure 2 The electric field spectrum of the intense electrostatic wave event shown in Figure 1. Notice the intense waves are sharply peaked at 56.2 kHz and the peak-to-average ratio is about 30, indicating large fluctuations in intensity on a time scale of a few seconds.

Figure 3 Another example of intense waves as measured by the IMP 6 instrument. This event is approximately 0.5 R_E outside the plasmapause. The magnetic spectrum analyzer data shown in the lower panel indicate the presence of a relatively small magnetic component for this event. The electric-to-magnetic field energy density ratio for this example is about 1600.

Figure 4 A display of all intense electrostatic wave events ($|E| \geq 1$ mV m^{-1}) detected during over five and one-half years of observations with the Hawkeye 1 and IMP 6 satellites. Each of four quadrants in magnetic local time are rotated into the noon-midnight and dawn-dusk magnetic meridian planes shown here. Notice the wide range of latitudes at which the intense waves are detected. The events also occur at all local times.

Figure 5 A series of histograms showing the number of intense electrostatic wave events with electric field amplitudes greater than about 1 mV m^{-1} as a function of radial distance. Each histogram represents the events detected at each of six different frequencies. The histogram labelled "~ 10 kHz" comprises events from IMP 6's 10-kHz channel and Hawkeye's 13.3-kHz channel and the histogram labelled "~ 17 kHz" combines the events from the 16.5- and 17.8-kHz channels from IMP 6 and Hawkeye 1, respectively. Notice the trend towards lower frequencies at greater distances, implying that the instability is closely related to either f_{UHR} or f_p^-.

Figure 6 a. A display of plasma wave measurements of an intense wave event detected by Hawkeye 1 with a summary of polarization measurements superimposed over the data. The spin modulation seen in many of the features has been analyzed to determine the orientation of the wave electric field with respect to the geomagnetic field. The shaded regions are regions of frequency and time where all waves are polarized such that $\vec{E} \| \vec{B}_o$, consistent with the polarization of nonthermal continuum radiation. The unshaded region indicates frequencies and times, including the intense electrostatic event at 31.1 kHz, when waves with measureable polarization have electric fields oriented perpendicular to $\vec{B}_o$. This polarization unambiguously identifies f_{UHR} as the characteristic frequency of the intense waves (see text). The hatched region consists of whistler-mode turbulence.

b. A display of plasma wave measurements of the same event shown in Figure 6a, but overlaid with lines at f_g^- and the lower order $(n + 1/2)f_g^-$ bands using the ordinate as a frequency scale. Notice that a large number of the features present in this complex region lie at or near the $(n + 1/2)f_g^-$ harmonics. In particular, the intense event at 31.1 kHz lies directly at the $7f_g^-/2$ harmonic.

Figure 7 A high-resolution frequency time spectrogram of intense electrostatic waves which occur not only at an $(n + 1/2)f_g^-$ harmonic, but also near f_{UHR}. The gyrofrequency for this event is about 1.9 kHz and f_{UHR} (using the lower frequency cutoff of the continuum radiation for f_p^-) is about 15.2 kHz.

Figure 8 A high latitude, intense electrostatic wave event to be compared to the plasma measurements shown in Plate 1. The time correlation between the presence of the intense waves in the 17.8-kHz channel and electron intensities near 1 keV is very good.

Figure 9 An intense electrostatic wave event at 100 kHz located near the magnetic equator. The energy-time spectrogram for plasma measurements gained during this event is shown on Plate 2.

Figure 10 An electrostatic wave event for which an electron velocity distribution has been measured and shown in Figure 11. The intense signal of interest occurs in the 17.8-kHz channel between about 0415 and 0435 UT.

Figure 11 A continuation of Figure 10 which presents the electron velocity distribution function from LEPEDEA observations in the period 0429 - 0433 UT on April 5, 1977. The area to the left of the dashed line through contours of constant $f(v_{\perp}, v_{\parallel})$ is a region at small $v_{\perp}$ for which the plasma analyzer responses are < 100 counts sec^{-1}.

Figure 12 The intense electrostatic wave event for which an electron velocity distribution has been measured and shown in Figure 13. This event, near 2345 UT in the 100-kHz channel, exhibits extreme fluctuations in amplitude on a time scale of minutes.

Figure 13 A continuation of Figure 12 which presents the electron velocity distribution function for the period 2346 - 2350 UT on November 17, 1975.

Figure 14 A continuation of Figure 9 and Plate 2 which presents the electron velocity distribution function for the period 2205 - 2207 UT on August 15, 1975.

Figure 15 Contours of constant phase-space density for a bi-Maxwellian distribution function with parameters $n_H = 0.125\ cm^{-3}$, $E_{\parallel} = 3$ keV, $E_{\perp} = 10$ keV, $\Delta = 0$ and $\beta = 0.9$ (solid lines) and the contours which result from the detection of that distribution with an analyzer whose field of view is the same as that for the Hawkeye LEPEDEA (dashed lines).

Figure 16 A demonstration of an intense electrostatic wave event as a local, compact source of nonthermal continuum radiation. Power flux plotted as a function of radial distance from the earth in the center panel does not show the R^{-2} dependence expected for a source centered at the earth. However, the plot of power flux as a function of the distance from the intense event centered at 4.3 R_E shows a definite $(R-R')^{-2}$ dependence.

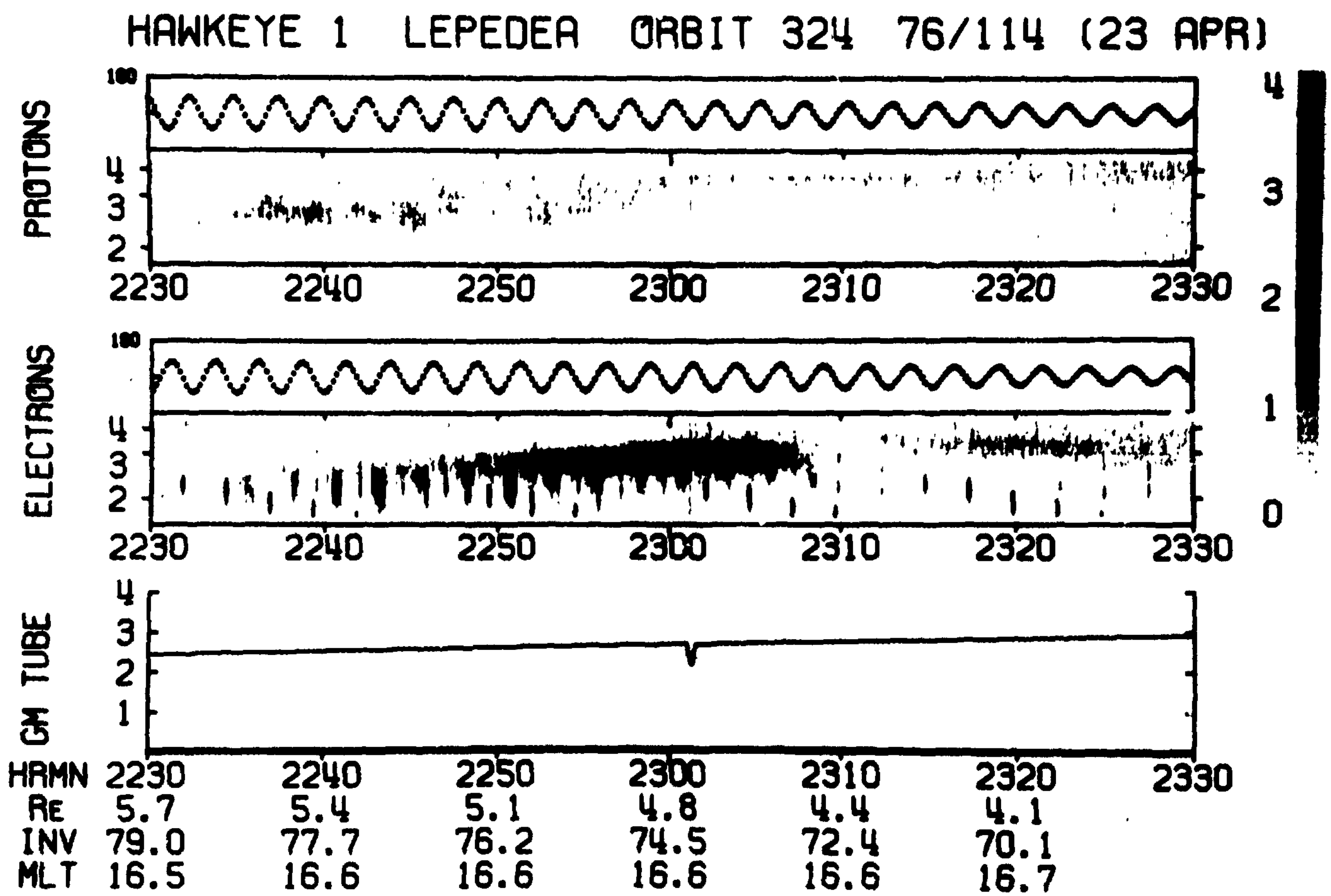
HAWKEYE 1 LEPEDEA ORBIT 324 76/114 (23 APR)
PROTONS
ELECTRONS
GM TUBE
HRMN 2230 2240 2250 2300 2310 2320 2330
RE 5.7 5.4 5.1 4.8 4.4 4.1
INV 79.0 77.7 76.2 74.5 72.4 70.1
MLT 16.5 16.6 16.6 16.6 16.6 16.7

Plate 1

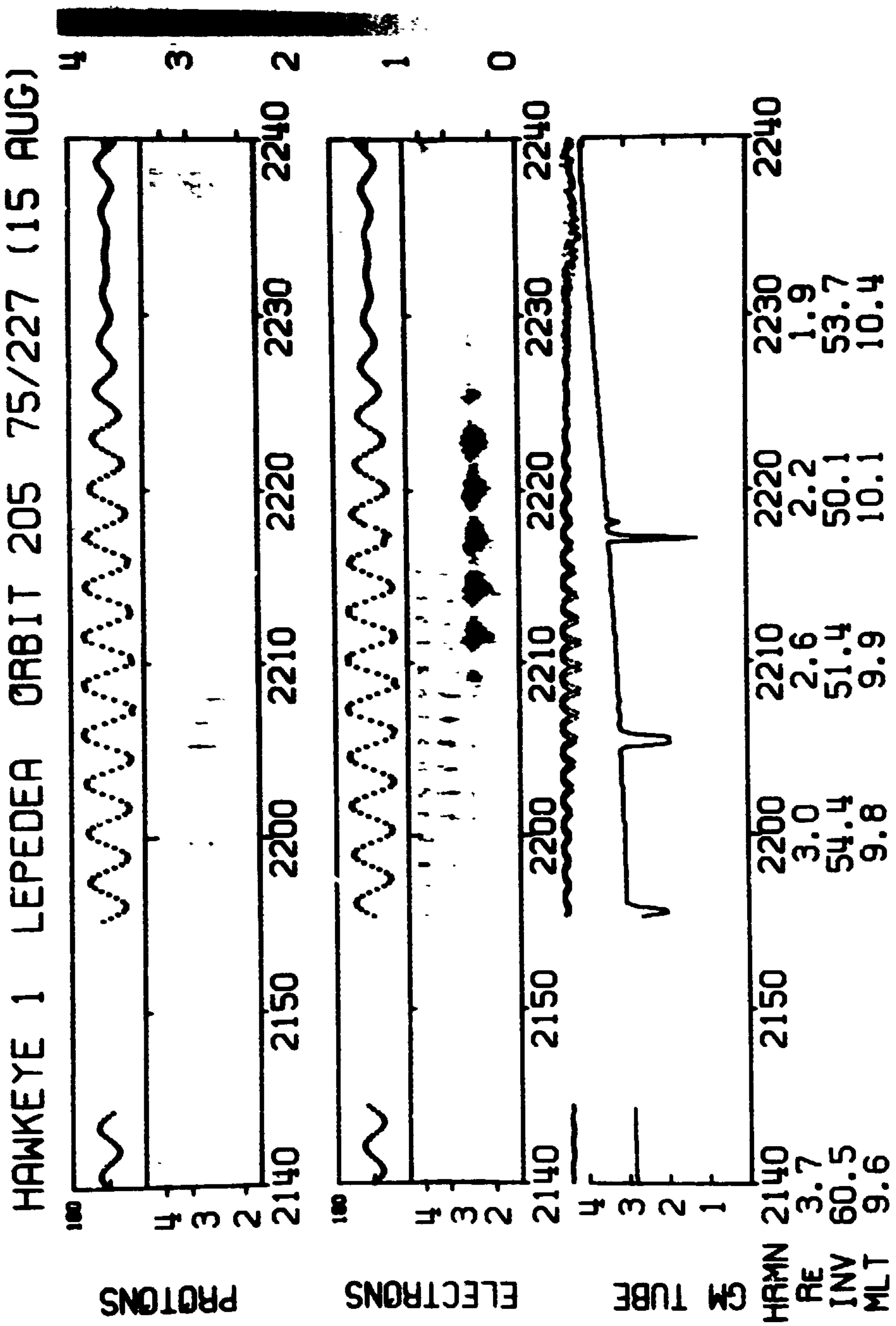
HAWKEYE 1 LEPEDEA ØRBIT 205 75/227 (15 AUG)
PROTONS
ELECTRONS
GM TUBE
HRMN 2140 2150 2200 2210 2220 2230 2240
RE 3.7 3.0 2.6 2.2 1.9
INV 60.5 54.4 51.4 50.1 53.7
MLT 9.6 9.8 9.9 10.1 10.4

Plate 2

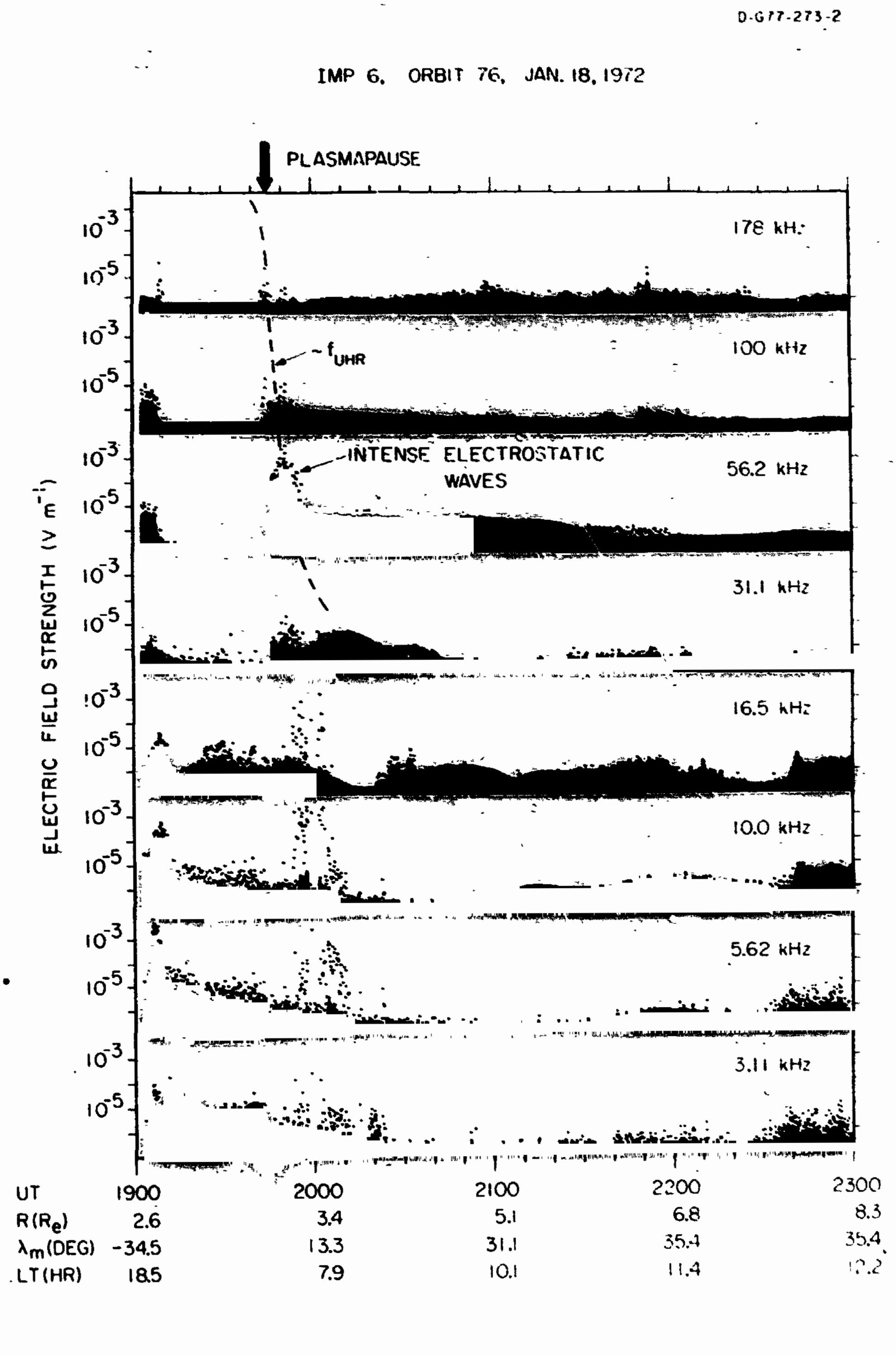
D-G77-273-2
IMP 6, ORBIT 76, JAN. 18, 1972
PLASMAPAUSE
178 kHz
100 kHz
~ f_{UHR}
INTENSE ELECTROSTATIC WAVES
56.2 kHz
31.1 kHz
16.5 kHz
10.0 kHz
5.62 kHz
3.11 kHz
ELECTRIC FIELD STRENGTH (V m^{-1})
10^{-3}
10^{-5}
UT 1900 2000 2100 2200 2300
R(R$_e$) 2.6 3.4 5.1 6.8 8.3
λ_m(DEG) -34.5 13.3 31.1 35.4 35.4
LT(HR) 18.5 7.9 10.1 11.4 12.2

Figure 1

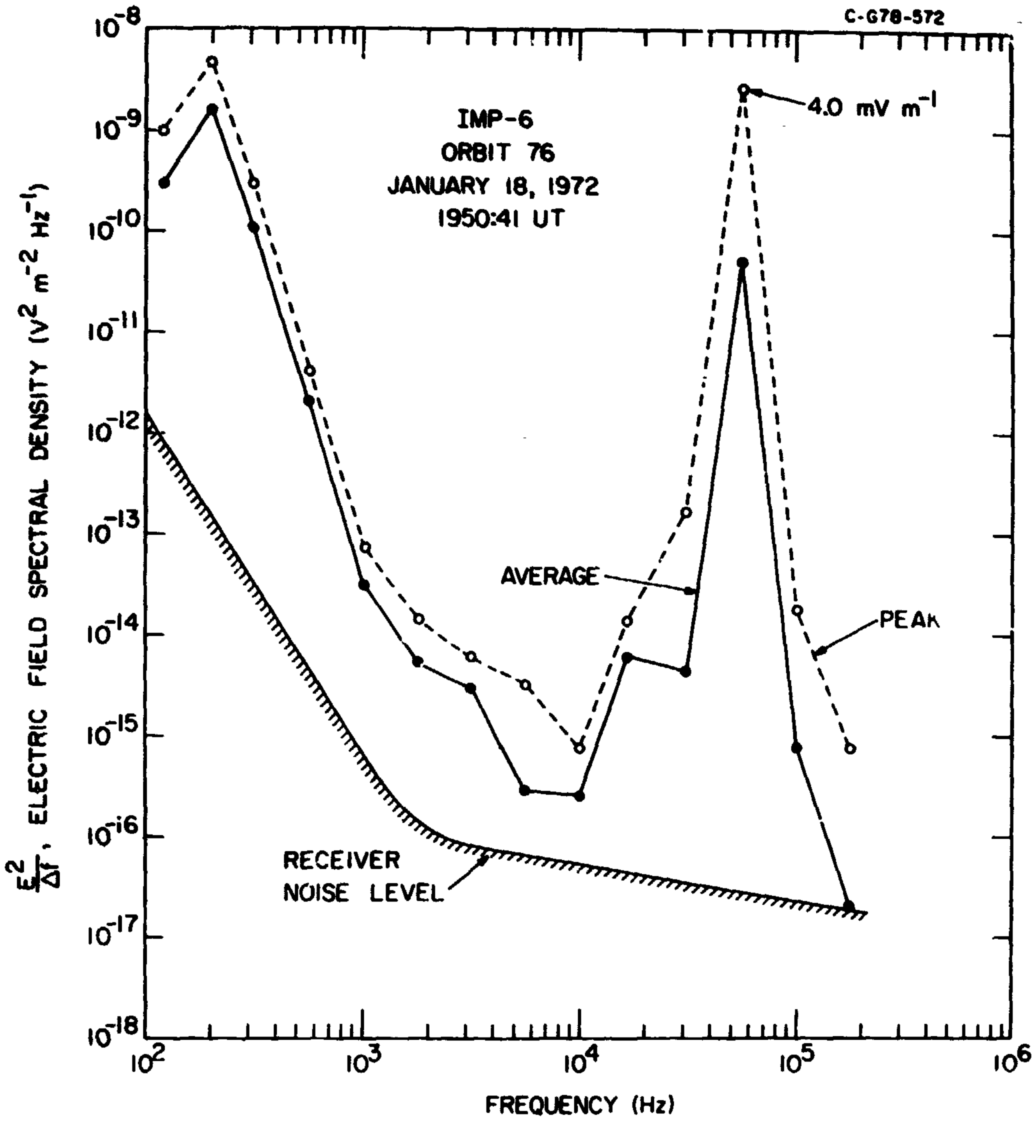
C-G78-572
IMP-6
ORBIT 76
JANUARY 18, 1972
1950:41 UT
4.0 mV m^{-1}
AVERAGE
PEAK
RECEIVER
NOISE LEVEL
$\frac{E^2}{\Delta f}$, ELECTRIC FIELD SPECTRAL DENSITY (V^2 m^{-2} Hz^{-1})
FREQUENCY (Hz)

Figure 2

D-G77-225-1

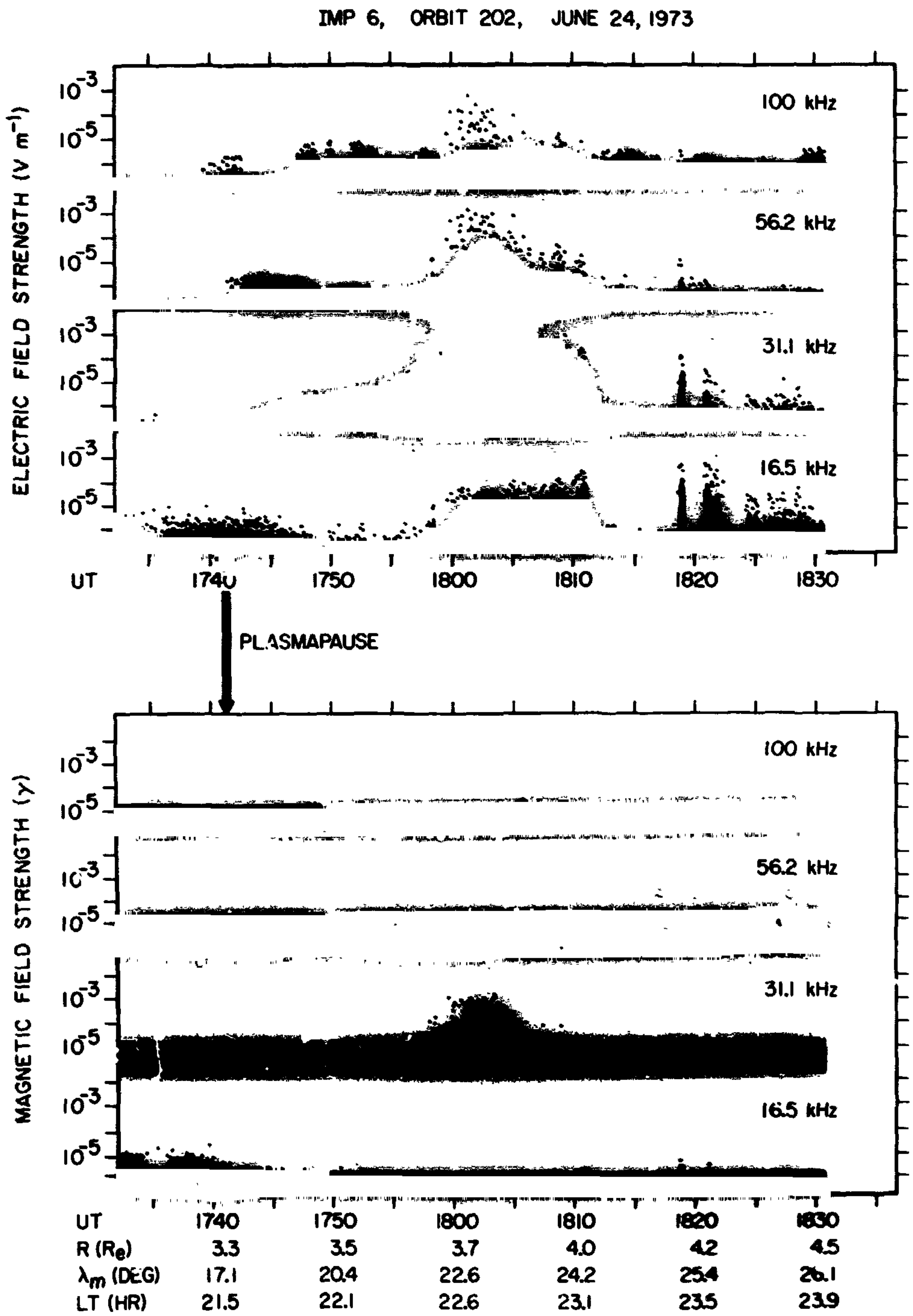

Figure 3

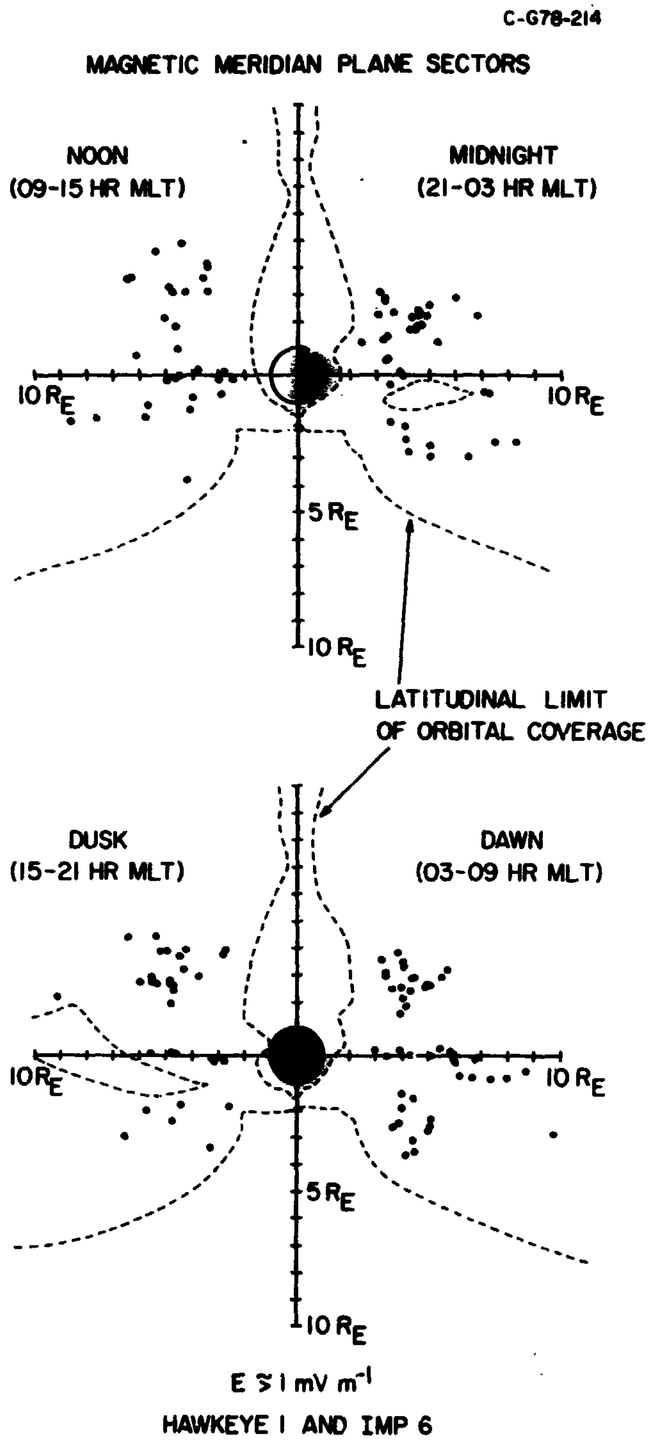
C-G78-214
MAGNETIC MERIDIAN PLANE SECTORS
NOON
(09-15 HR MLT)
MIDNIGHT
(21-03 HR MLT)
10 R_E
10 R_E
5 R_E
10 R_E
LATITUDINAL LIMIT
OF ORBITAL COVERAGE
DUSK
(15-21 HR MLT)
DAWN
(03-09 HR MLT)
10 R_E
10 R_E
5 R_E
10 R_E
$E \gtrsim 1$ mV m^{-1}
HAWKEYE I AND IMP 6

Figure 4

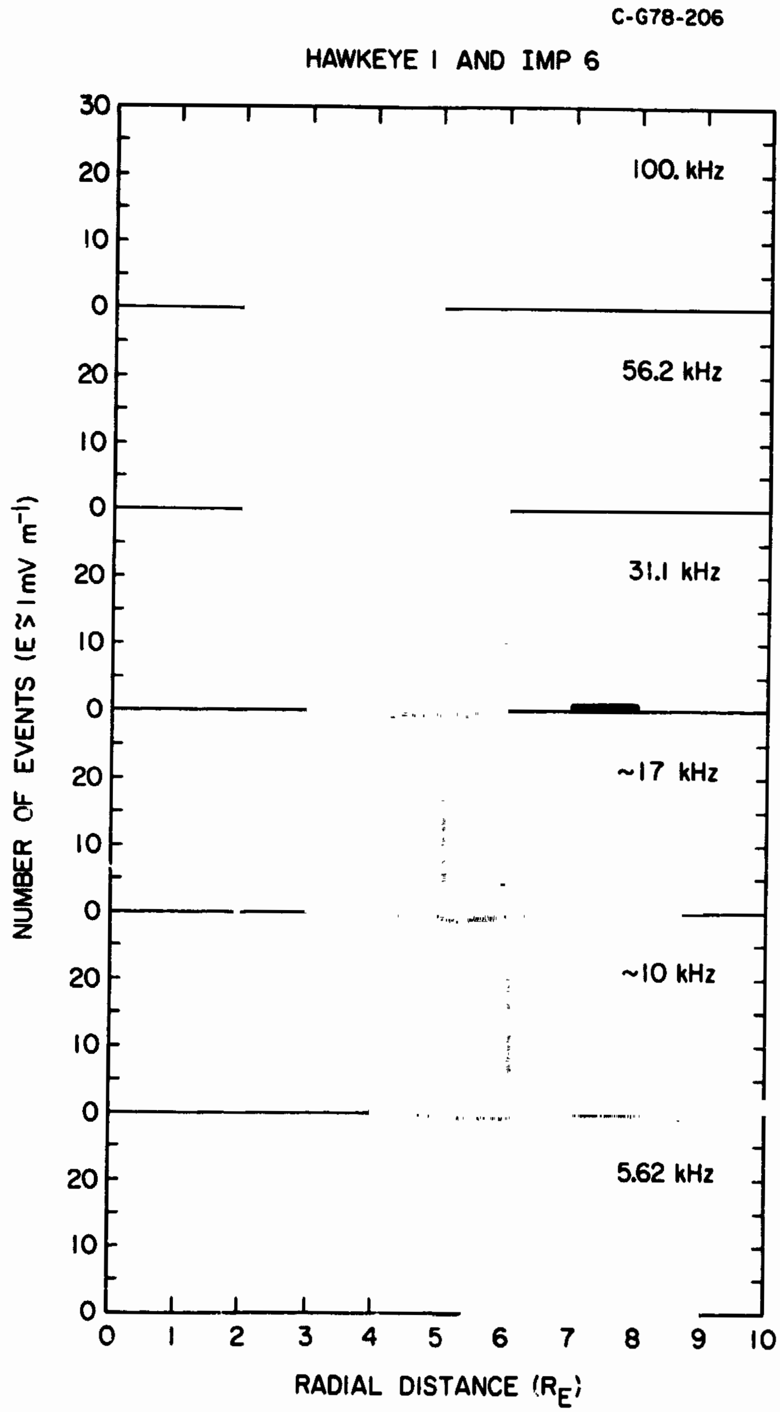
C-G78-206
HAWKEYE I AND IMP 6
100. kHz
56.2 kHz
31.1 kHz
~17 kHz
~10 kHz
5.62 kHz
NUMBER OF EVENTS (E ≳ 1 mV m⁻¹)
RADIAL DISTANCE (R_E)

Figure 5

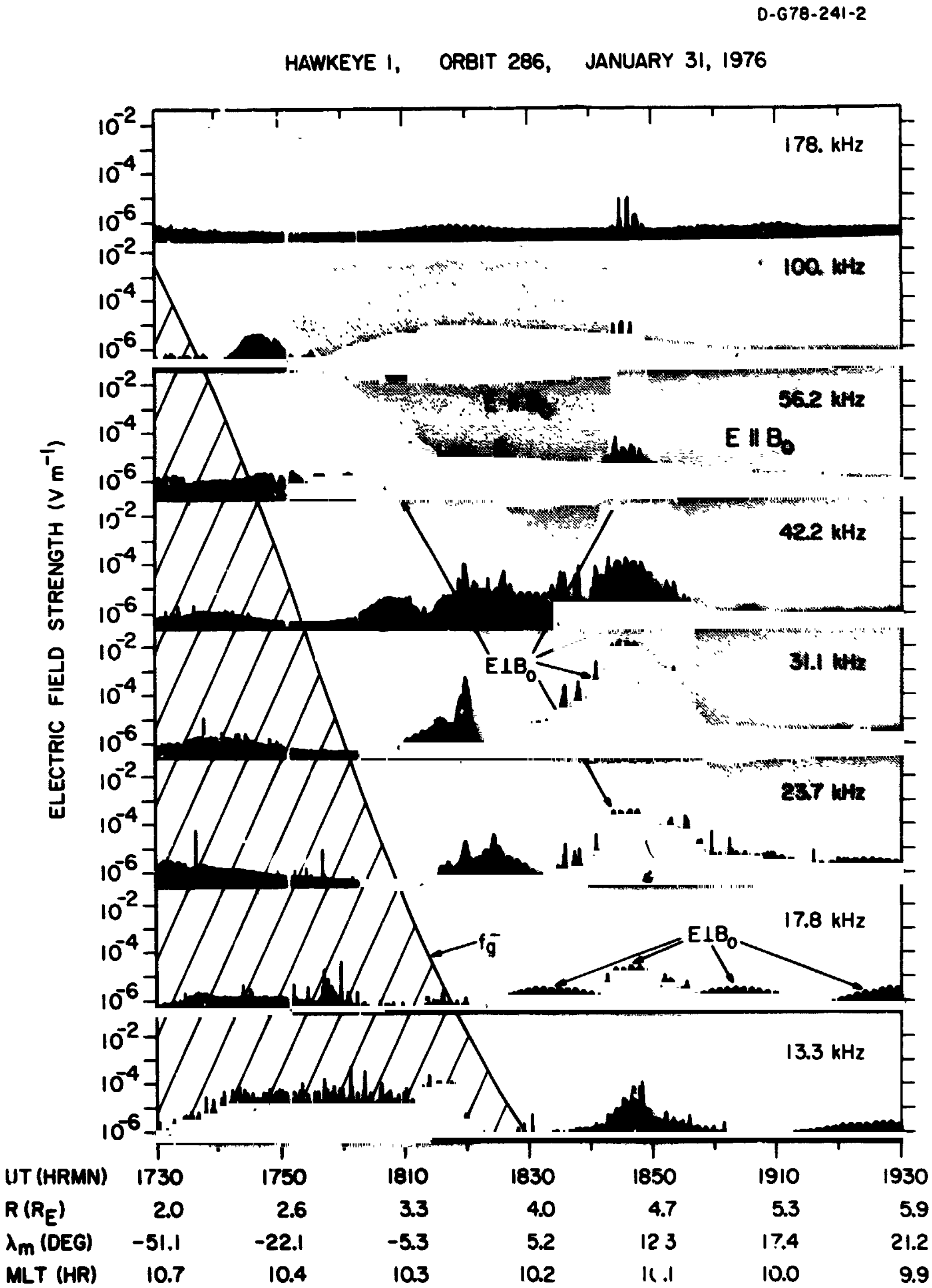
D-G78-241-2
HAWKEYE I, ORBIT 286, JANUARY 31, 1976
ELECTRIC FIELD STRENGTH (V m^{-1})
178. kHz
100. kHz
56.2 kHz
E ∥ B$_0$
42.2 kHz
E⊥B$_0$
31.1 kHz
23.7 kHz
17.8 kHz
E⊥B$_0$
f_g^-
13.3 kHz
10^{-2}
10^{-4}
10^{-6}
UT (HRMN) 1730 1750 1810 1830 1850 1910 1930
R (R$_E$) 2.0 2.6 3.3 4.0 4.7 5.3 5.9
λ$_m$ (DEG) -51.1 -22.1 -5.3 5.2 12.3 17.4 21.2
MLT (HR) 10.7 10.4 10.3 10.2 10.1 10.0 9.9

Figure 6a

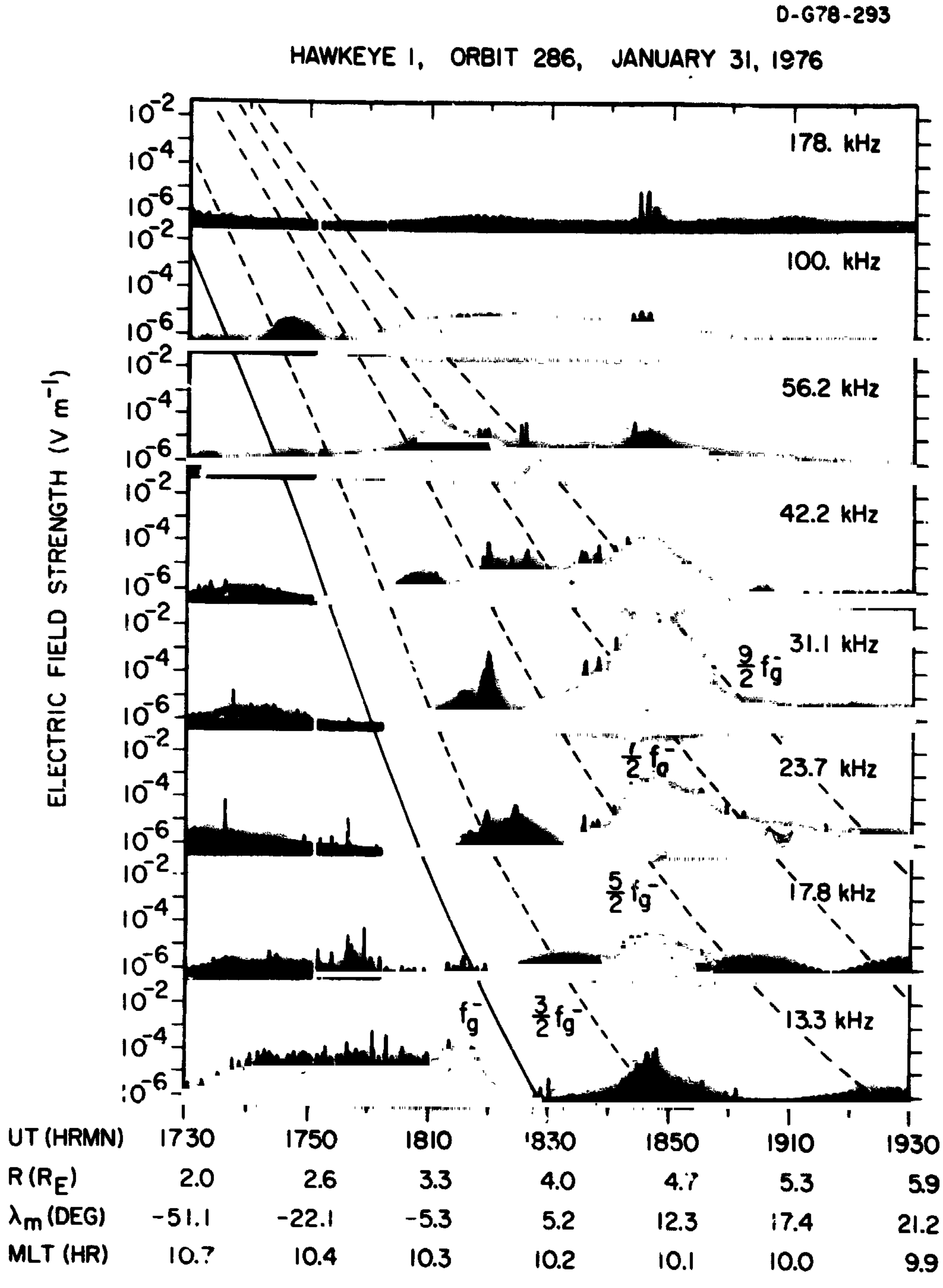
D-G78-293
HAWKEYE I, ORBIT 286, JANUARY 31, 1976
ELECTRIC FIELD STRENGTH (V m⁻¹)
178. kHz
100. kHz
56.2 kHz
42.2 kHz
31.1 kHz
23.7 kHz
17.8 kHz
13.3 kHz
9/2 f_g⁻
7/2 f_g⁻
5/2 f_g⁻
3/2 f_g⁻
f_g⁻
UT (HRMN) 1730 1750 1810 1830 1850 1910 1930
R (R_E) 2.0 2.6 3.3 4.0 4.7 5.3 5.9
λm (DEG) -51.1 -22.1 -5.3 5.2 12.3 17.4 21.2
MLT (HR) 10.7 10.4 10.3 10.2 10.1 10.0 9.9

Figure 6b

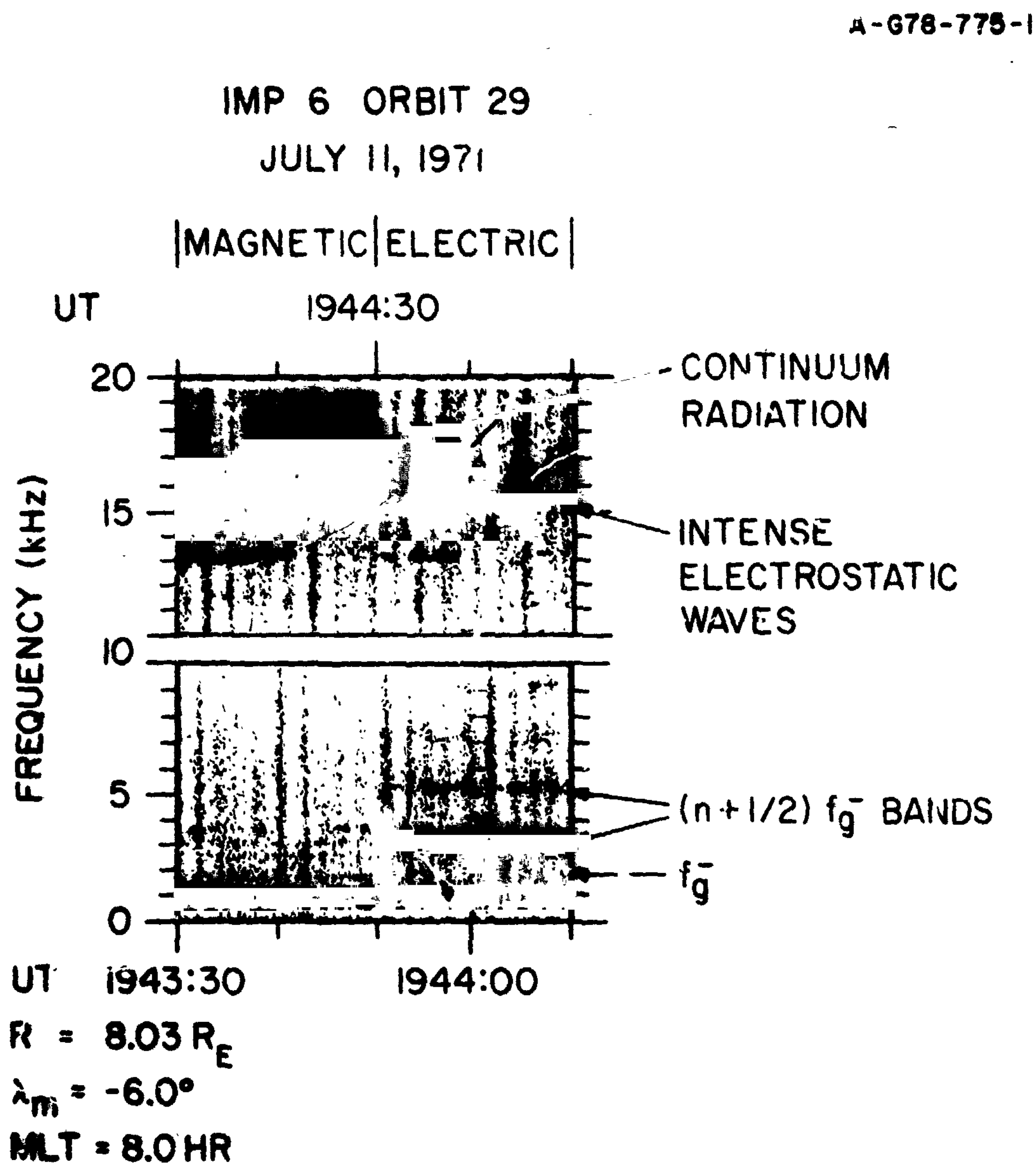
A-G78-775-1
IMP 6 ORBIT 29
JULY 11, 1971
MAGNETIC
ELECTRIC
UT
1944:30
20
15
10
5
0
FREQUENCY (kHz)
CONTINUUM RADIATION
INTENSE ELECTROSTATIC WAVES
(n+1/2) fg⁻ BANDS
fg⁻
UT
1943:30
1944:00
R = 8.03 RE
λm = -6.0°
MLT = 8.0 HR

Figure 7

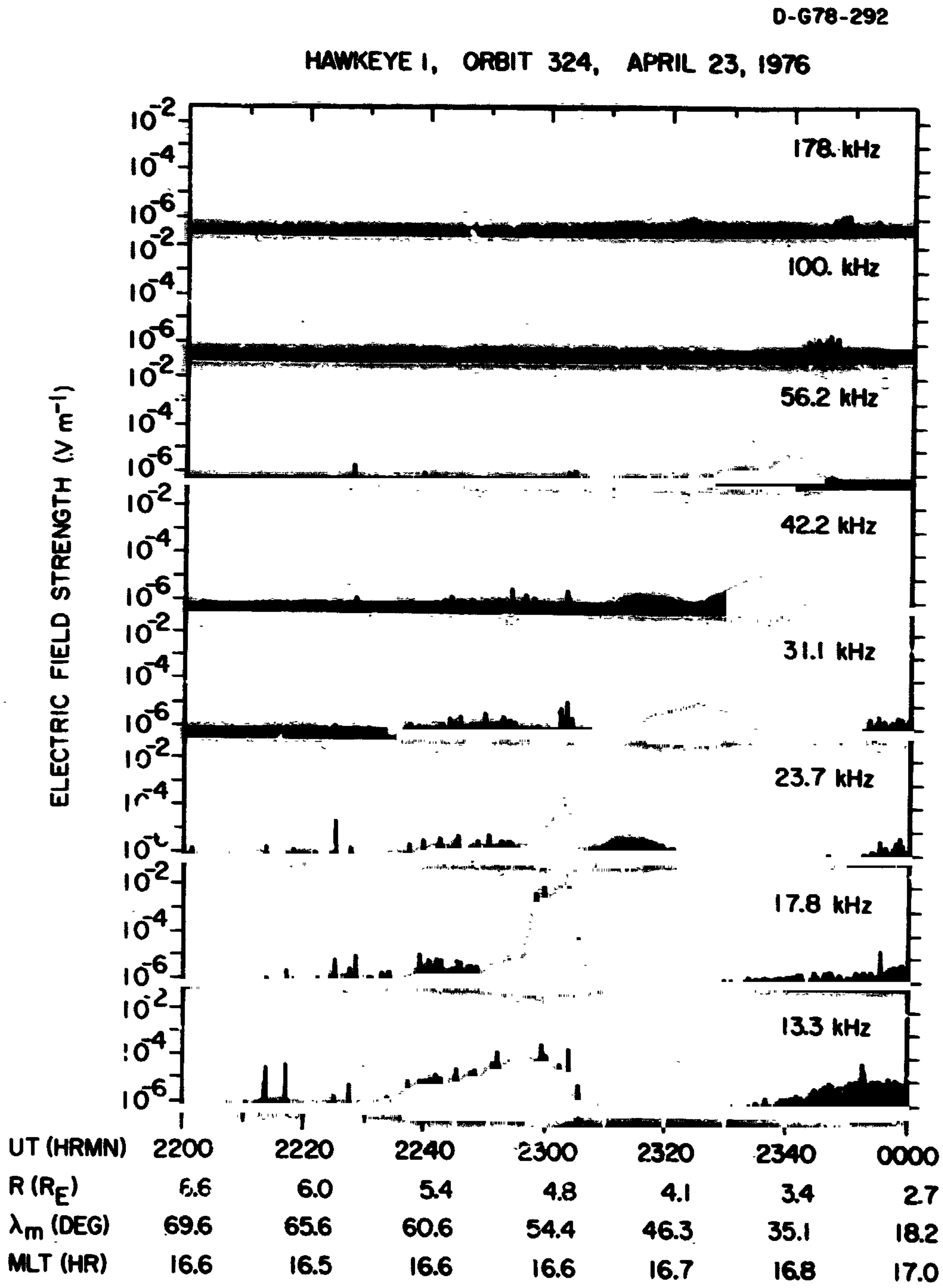
D-G78-292
HAWKEYE I, ORBIT 324, APRIL 23, 1976
178. kHz
100. kHz
56.2 kHz
42.2 kHz
31.1 kHz
23.7 kHz
17.8 kHz
13.3 kHz
ELECTRIC FIELD STRENGTH (V m⁻¹)
UT (HRMN) 2200 2220 2240 2300 2320 2340 0000
R (RE) 6.6 6.0 5.4 4.8 4.1 3.4 2.7
λm (DEG) 69.6 65.6 60.6 54.4 46.3 35.1 18.2
MLT (HR) 16.6 16.5 16.6 16.6 16.7 16.8 17.0

Figure 8

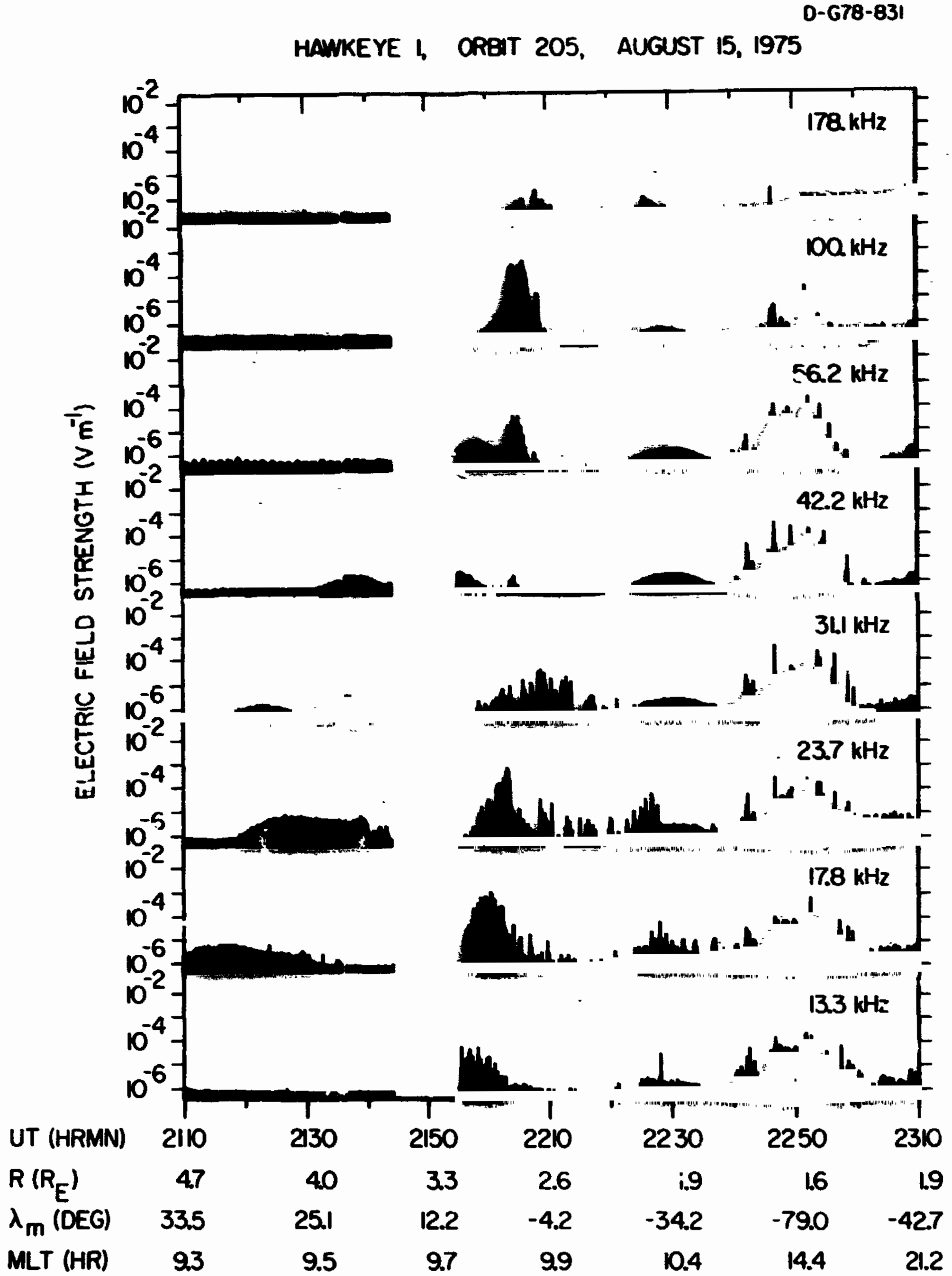
D-G78-831
HAWKEYE 1, ORBIT 205, AUGUST 15, 1975
178 kHz
100 kHz
56.2 kHz
42.2 kHz
31.1 kHz
23.7 kHz
17.8 kHz
13.3 kHz
ELECTRIC FIELD STRENGTH (V m-1)
UT (HRMN) 2110 2130 2150 2210 2230 2250 2310
R (RE) 4.7 4.0 3.3 2.6 1.9 1.6 1.9
λm (DEG) 33.5 25.1 12.2 -4.2 -34.2 -79.0 -42.7
MLT (HR) 9.3 9.5 9.7 9.9 10.4 14.4 21.2

Figure 9

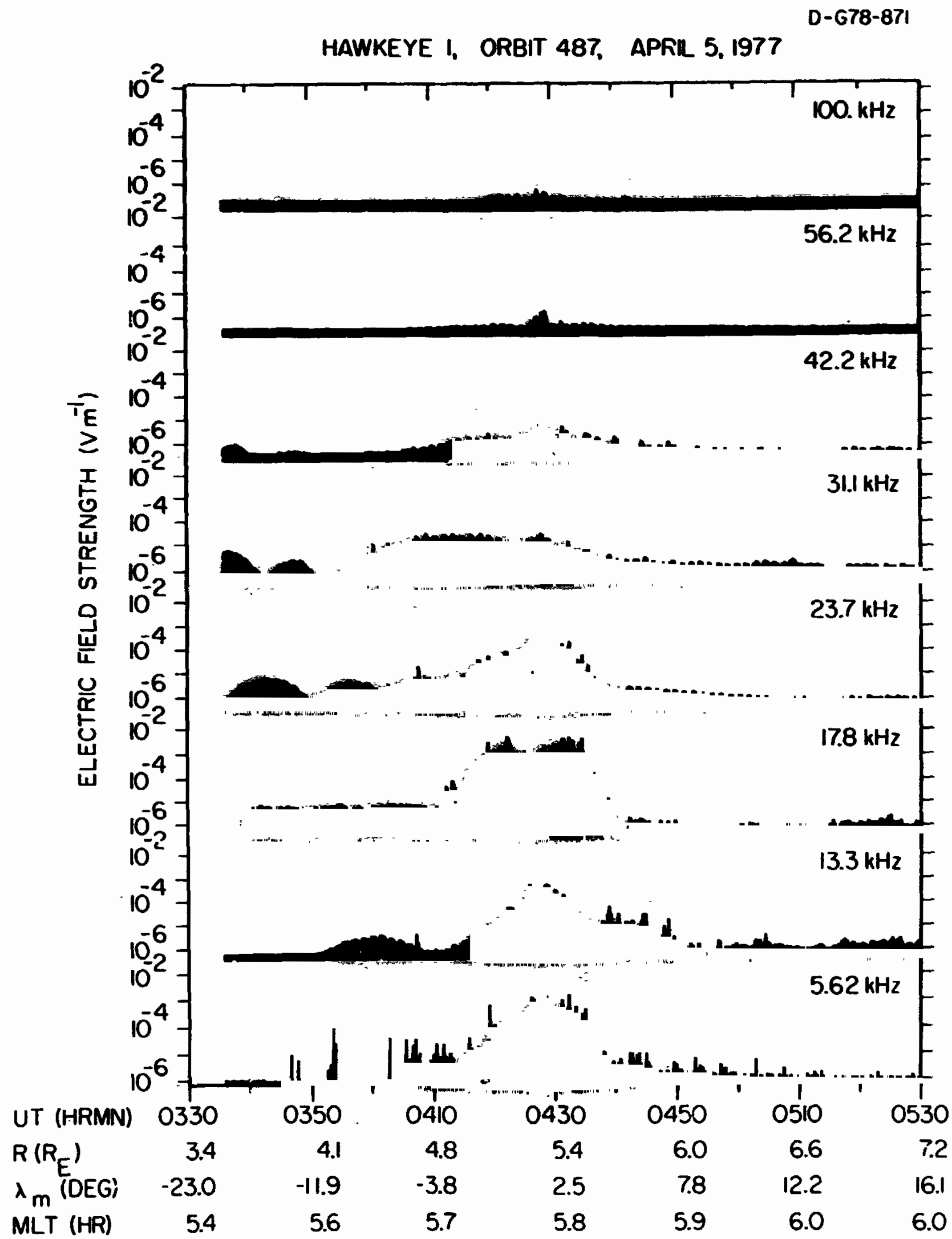
D-G78-871
HAWKEYE I, ORBIT 487, APRIL 5, 1977
100. kHz
56.2 kHz
42.2 kHz
31.1 kHz
23.7 kHz
17.8 kHz
13.3 kHz
5.62 kHz
ELECTRIC FIELD STRENGTH (V m⁻¹)
10⁻²
10⁻⁴
10⁻⁶
UT (HRMN) 0330 0350 0410 0430 0450 0510 0530
R (R_E) 3.4 4.1 4.8 5.4 6.0 6.6 7.2
λ_m (DEG) -23.0 -11.9 -3.8 2.5 7.8 12.2 16.1
MLT (HR) 5.4 5.6 5.7 5.8 5.9 6.0 6.0

Figure 10

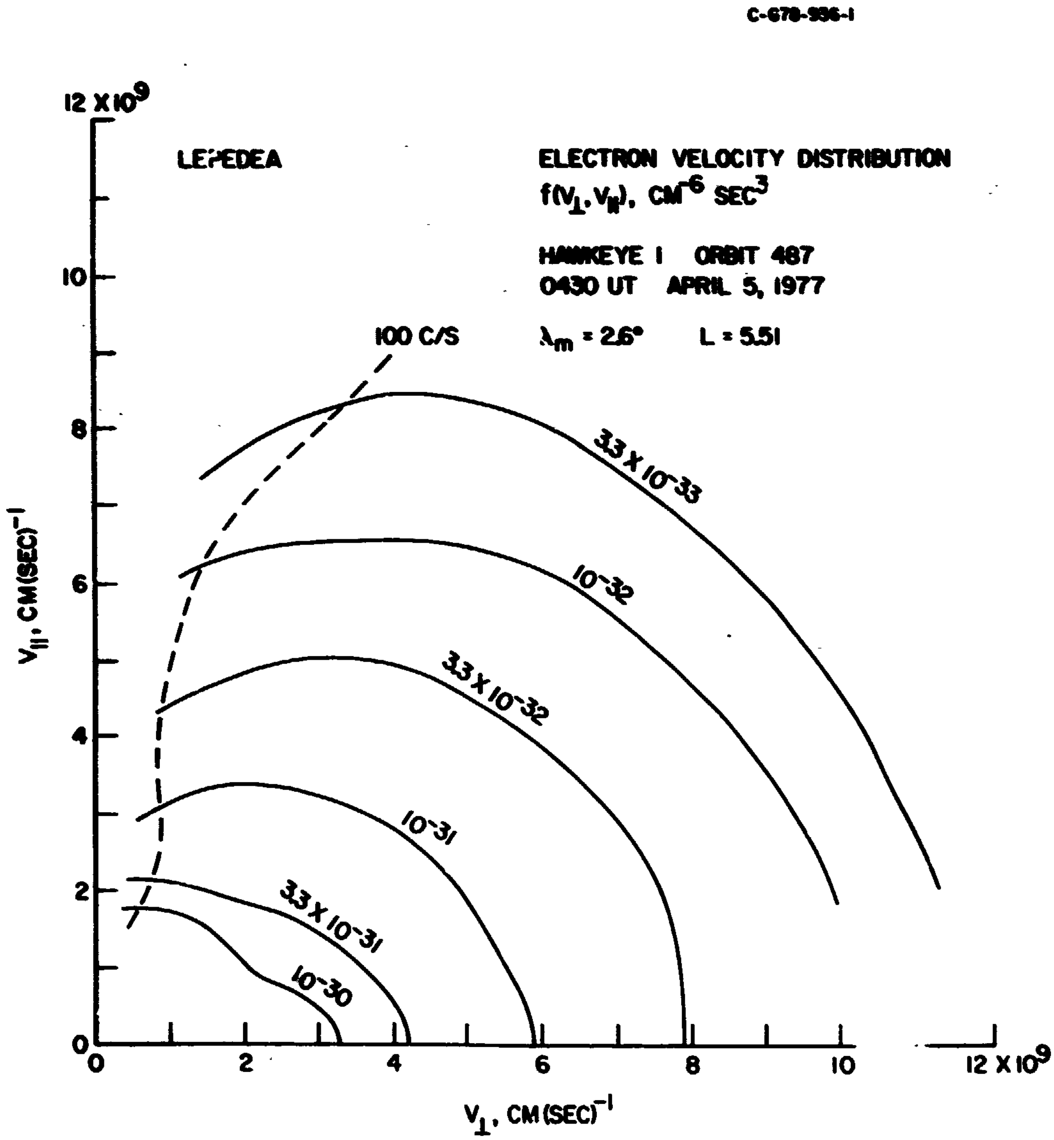
C-G78-936-1
LEPEDEA
ELECTRON VELOCITY DISTRIBUTION
f(V⊥,V∥), CM-6 SEC3
HAWKEYE I ORBIT 487
0430 UT APRIL 5, 1977
λm = 2.6° L = 5.51
100 C/S
3.3 X 10-33
10-32
3.3 X 10-32
10-31
3.3 X 10-31
10-30
12 X 10^9
10
8
6
4
2
0
0
2
4
6
8
10
12 X 10^9
V∥, CM(SEC)-1
V⊥, CM(SEC)-1

Figure 11

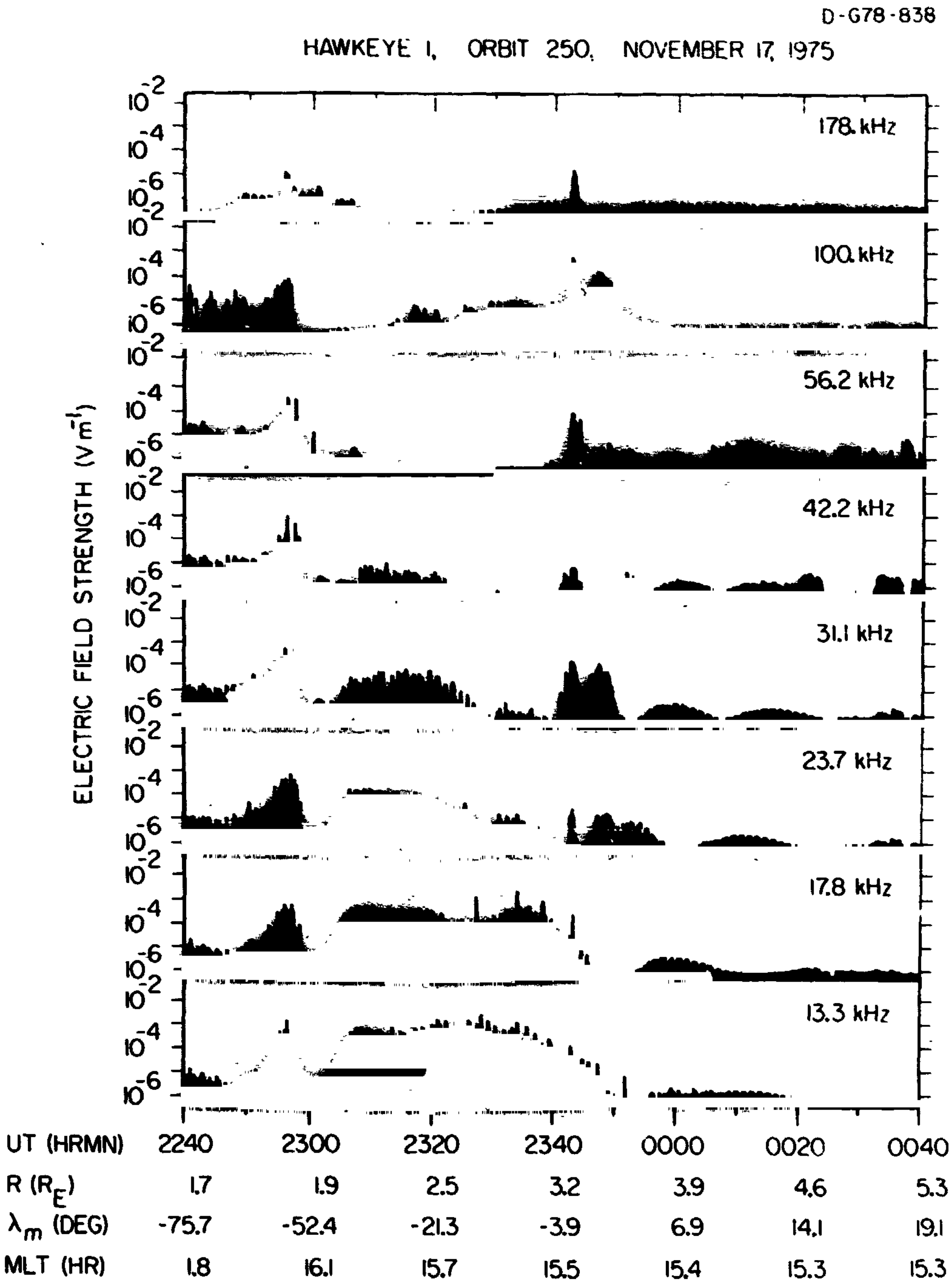
D-G78-838
HAWKEYE 1, ORBIT 250, NOVEMBER 17, 1975
178 kHz
100 kHz
56.2 kHz
42.2 kHz
31.1 kHz
23.7 kHz
17.8 kHz
13.3 kHz
ELECTRIC FIELD STRENGTH (V m⁻¹)
10⁻²
10⁻⁴
10⁻⁶
UT (HRMN) 2240 2300 2320 2340 0000 0020 0040
R (R_E) 1.7 1.9 2.5 3.2 3.9 4.6 5.3
λ_m (DEG) -75.7 -52.4 -21.3 -3.9 6.9 14.1 19.1
MLT (HR) 1.8 16.1 15.7 15.5 15.4 15.3 15.3

Figure 12

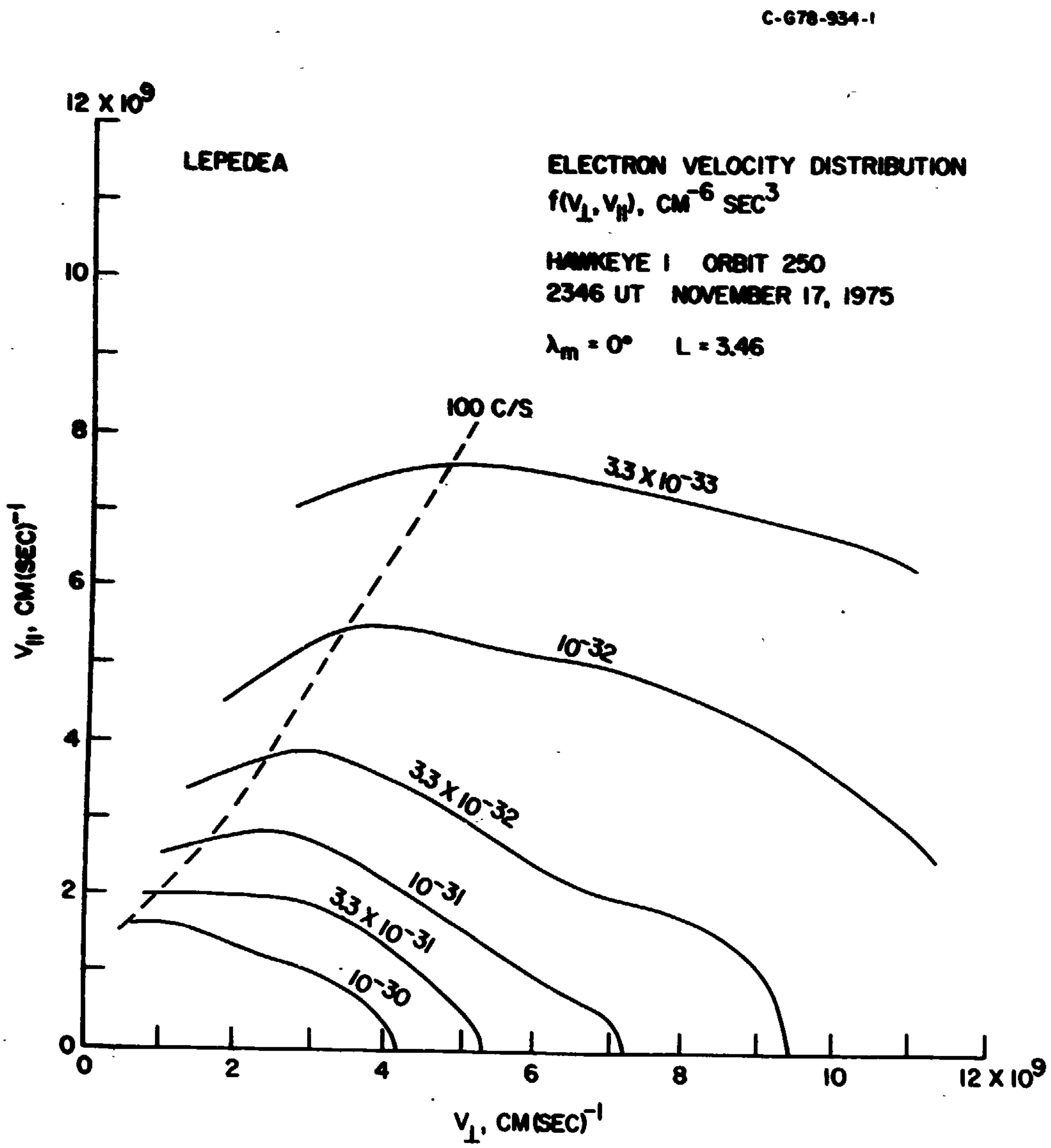
C-G78-934-1
LEPEDEA
ELECTRON VELOCITY DISTRIBUTION
f(V⊥, V∥), CM⁻⁶ SEC³
HAWKEYE I ORBIT 250
2346 UT NOVEMBER 17, 1975
λm = 0° L = 3.46
100 C/S
3.3 X 10⁻³³
10⁻³²
3.3 X 10⁻³²
10⁻³¹
3.3 X 10⁻³¹
10⁻³⁰
V∥, CM(SEC)⁻¹
V⊥, CM(SEC)⁻¹
12 X 10⁹
0
2
4
6
8
10

Figure 13

C-G78-933-2

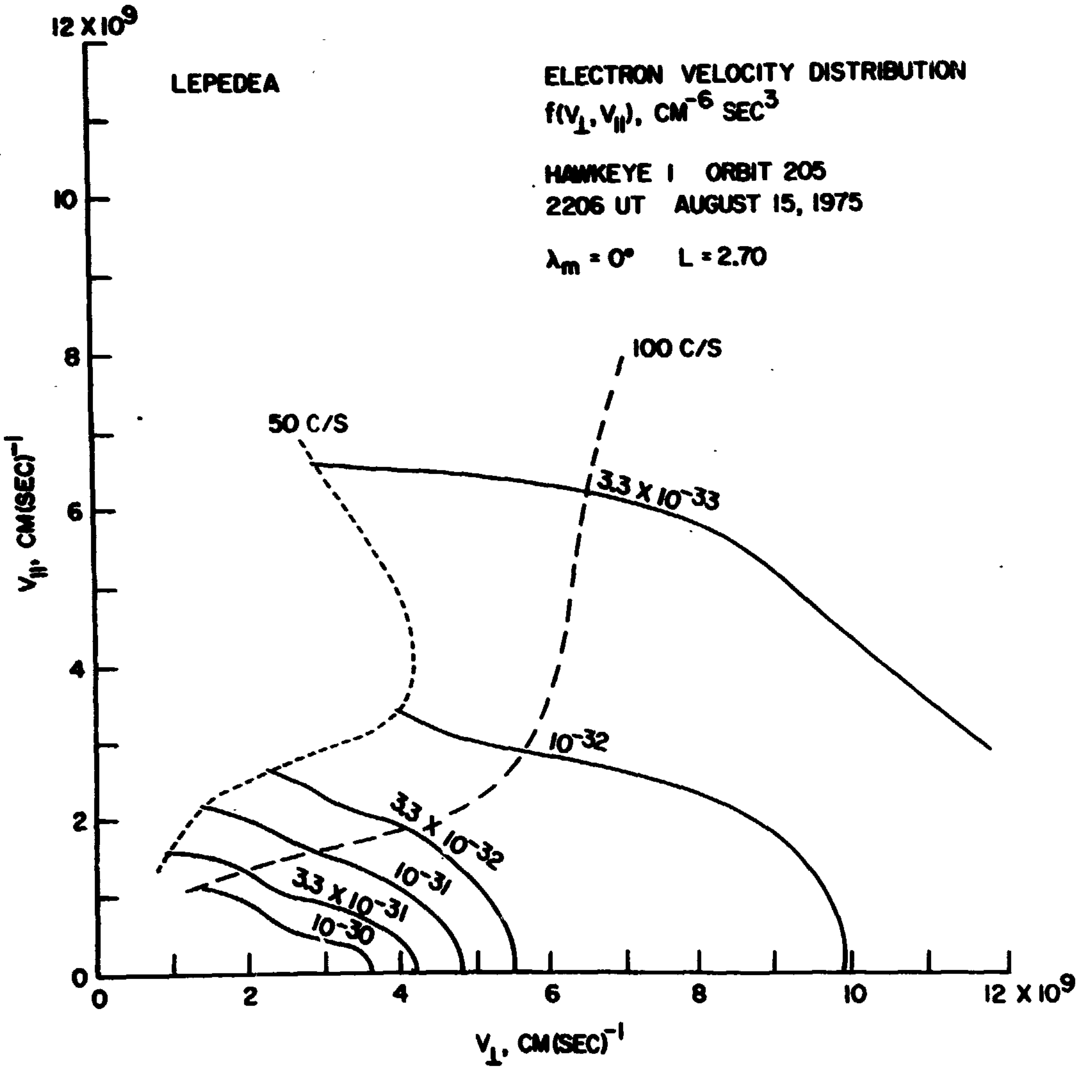

Figure 14

C-G78-998

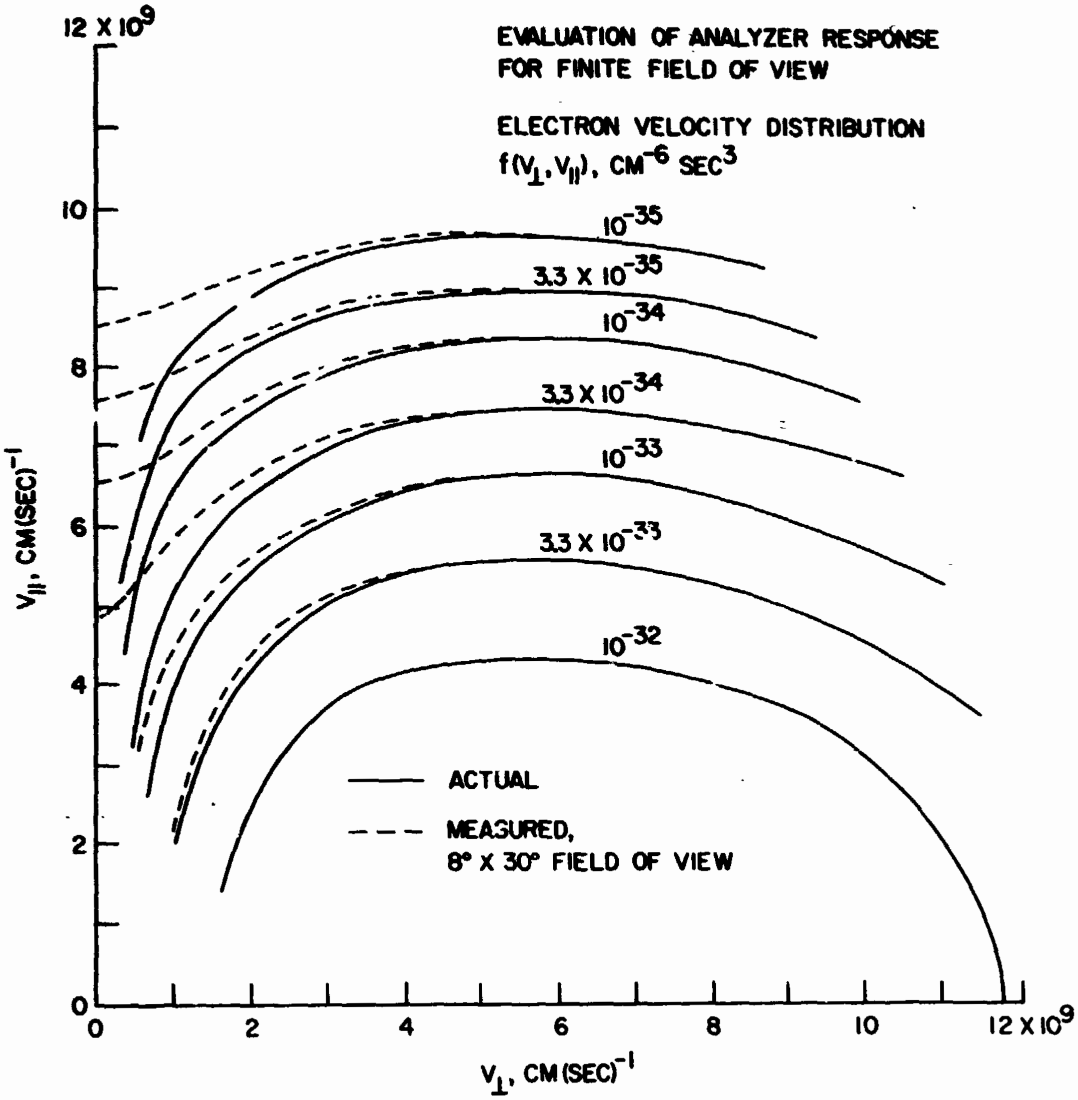

Figure 15

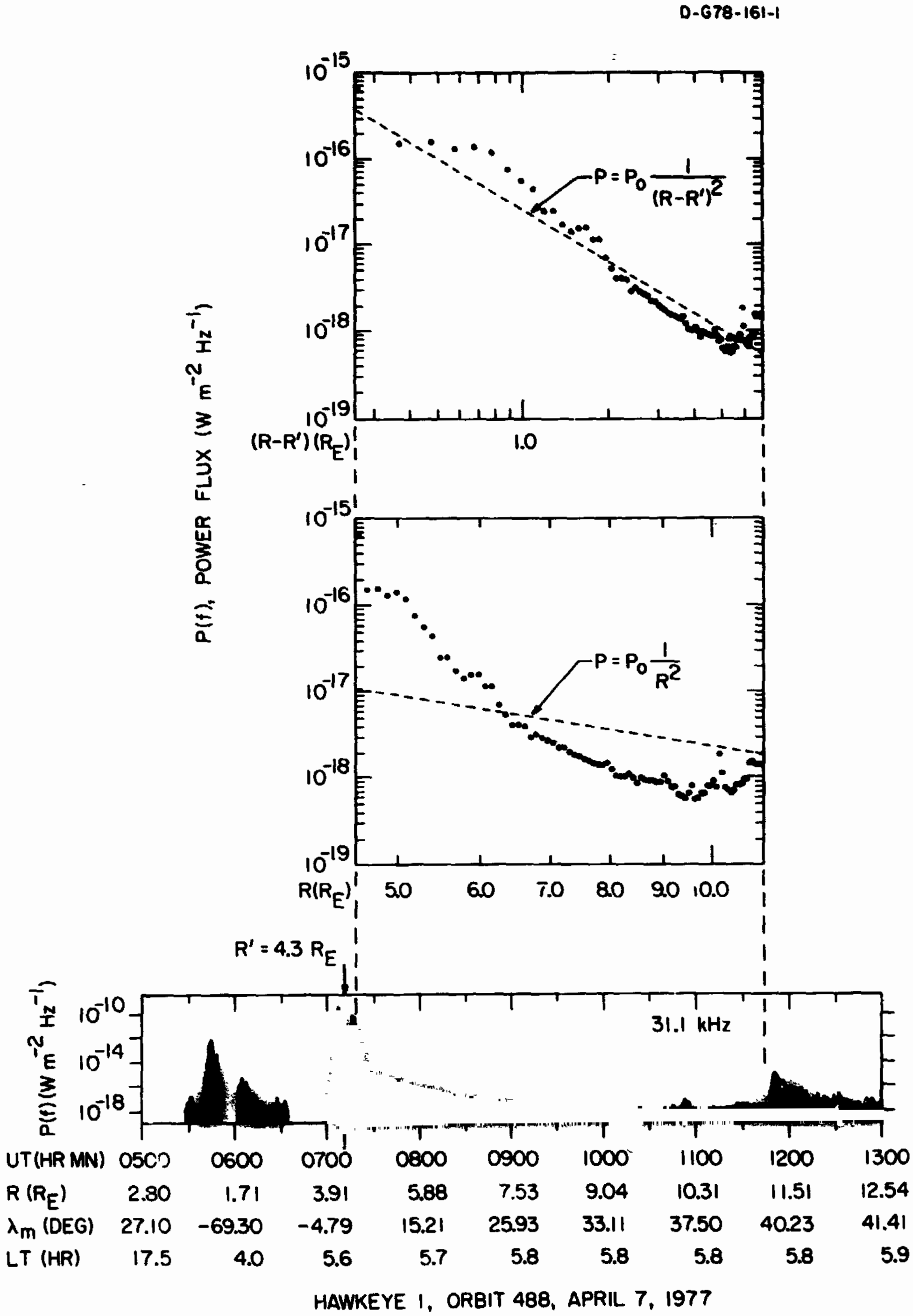
D-G78-161-1
$P = P_0 \frac{1}{(R-R')^2}$
$P = P_0 \frac{1}{R^2}$
P(f), POWER FLUX (W m^{-2} Hz^{-1})
(R-R') (R$_E$)
1.0
R(R$_E$)
5.0
6.0
7.0
8.0
9.0
10.0
R' = 4.3 R$_E$
31.1 kHz
P(f) (W m^{-2} Hz^{-1})
UT (HR MN) 0500 0600 0700 0800 0900 1000 1100 1200 1300
R (R$_E$) 2.80 1.71 3.91 5.88 7.53 9.04 10.31 11.51 12.54
λ_m (DEG) 27.10 -69.30 -4.79 15.21 25.93 33.11 37.50 40.23 41.41
LT (HR) 17.5 4.0 5.6 5.7 5.8 5.8 5.8 5.8 5.9
HAWKEYE 1, ORBIT 488, APRIL 7, 1977

Figure 16